Pure Appl. Geophys. 167 (2010), 1013–1048

DOI 10.1007/s00024-010-0085-1

Pure and Applied Geophysics

Seismic Hazard Evaluation in Western Turkey as Revealed by Stress Transfer and Time-dependent Probability Calculations

P. M. Paradisopoulou,[1] E. E. Papadimitriou,[1] V. G. Karakostas,[1] T. Taymaz,[2] A. Kilias,[3] and S. Yolsal[2]

Abstract—Western Turkey has a long history of destructive earthquakes that are responsible for the death of thousands of people and which caused devastating damage to the existing infrastructures, and cultural and historical monuments. The recent earthquakes of Izmit (Kocaeli) on 17 August, 1999 ($M_w = 7.4$) and Düzce ($M_w = 7.2$) on 12 November, 1999, which occurred in the neighboring fault segments along the North Anatolian Fault (NAF), were catastrophic ones for the Marmara region and surroundings in NW Turkey. Stress transfer between the two adjacent fault segments successfully explained the temporal proximity of these events. Similar evidence is also provided from recent studies dealing with successive strong events occurrence along the NAF and parts of the Aegean Sea; in that changes in the stress field due to the coseismic displacement of the stronger events influence the occurrence of the next events of comparable size by advancing their occurrence time and delimiting their occurrence place. In the present study the evolution of the stress field since the beginning of the twentieth century in the territory of the eastern Aegean Sea and western Turkey is examined, in an attempt to test whether the history of cumulative changes in stress can explain the spatial and temporal occurrence patterns of large earthquakes in this area. Coulomb stress changes are calculated assuming that earthquakes can be modeled as static dislocations in elastic half space, taking into account both the coseismic slip in large ($M \geq 6.5$) earthquakes and the slow tectonic stress buildup along the major fault segments. The stress change calculations were performed for strike-slip and normal faults. In each stage of the evolutionary model the stress field is calculated according to the strike, dip, and rake angles of the next large event, whose triggering is inspected, and the possible sites for future strong earthquakes can be assessed. A new insight on the evaluation of future seismic hazards is given by translating the calculated stress changes into earthquake probability using an earthquake nucleation constitutive relation, which includes permanent and transient effects of the sudden stress changes.

Key words: Stress transfer, earthquake probabilities, seismic hazard.

1. Introduction

Many destructive earthquakes occurred in the territory of western Turkey and the adjacent eastern part of the Aegean Sea, some of them close both in time and space. Observations on temporal and spatial clustering of strong events have led several authors to highlight the importance of fault interactions on the basis of physical models. Earthquake triggering or delay due to changes in stress was recognized more than a decade ago (e.g., Harris, 1998 and references therein) and is worked out in assessing earthquake occurrence and future seismic hazard in a certain area. Stein (1999), reviewing the role of stress transfer, emphasized the earthquake interaction as a fundamental feature of seismicity that promises a deeper understanding of the earthquake occurrence and a better description of the seismic hazard, when stress transfer is incorporated into probability models (Stein *et al.*, 1997; Toda *et al.*, 1998). In association with physical fault models and fault properties, such models were more developed and statistically assessed (Parsons, 2004, 2005; Hardebeck, 2004; among others).

The first goal of the present study is to investigate how the stress changes caused by the strong earthquakes of $M \geq 6.5$ that occurred during the instrumental era, that is since the beginning of the twentieth century in the area of eastern Aegean Sea

[1] Department of Geophysics, School of Geology, Aristotle University of Thessaloniki, 54124 Thessaloniki, Greece. E-mail: popi.paradis@gmail.com; ritsa@geo.auth.gr; vkarak@geo.auth.gr

[2] Department of Geophysics, The Faculty of Mines, İstanbul Technical University, Maslak, 34469 Istanbul, Turkey. E-mail: taymaz@itu.edu.tr; yolsalse@itu.edu.tr

[3] Department of Geology, School of Geology, Aristotle University of Thessaloniki, 54124 Thessaloniki, Greece. E-mail: kilias@geo.auth.gr

and western Turkey (Fig. 1), influence future occurrences. This is attempted by the application of the stress evolutionary model (DENG and SYKES, 1997) according to which the long-term tectonic loading on the major regional faults is added to the coseismic slips of the strong events. As a second step the static stress changes on specific faults that have accumulated to date will be incorporated into probabilistic models, in an attempt to assess the seismic hazard in the study area. The first relevant investigation along the North Anatolian Fault was compiled by STEIN *et al.* (1997) who found that 9 out of 10 earthquakes with $M \geq 6.7$ were triggered by previous events, and estimated stress-based probabilities. Investigation of stress transfer in northwestern Turkey and the North Aegean Sea was performed by NALBANT *et al.* (1998) by the calculation of the static stress changes due to the coseismic slips of $M \geq 6.0$ events, whereas PAPADIMITRIOU and SYKES (2001) applied the stress evolutionary model in the Northern Aegean Sea for strike-slip faulting. HUBERT-FERRARI *et al.* (2000) calculated the stress field that resulted from the coseismic slips of events of M 6 or greater since 1700 and the secular interseismic stress changes to show that the 1999 events were anticipated. For the southeastern Aegean area, part of which coincides partially with our study area, the evolutionary model satisfactorily explained the clustering of strong ($M \geq 6.5$) normal faulting earthquakes (PAPADIMITRIOU *et al.*, 2005). In all these studies possible future occurrences are suggested, which will be discussed in the following sections along with the results obtained in the present study.

This study differs from the previously mentioned ones, as regards calculations of static stress changes, in that it aims to integrate the stress evolution history of the entire territory of western Turkey and its adjacent Aegean Sea area. This integration concerns both the areal coverage and the involvement of different faulting types and the continuous tectonic loading, since the above-mentioned studies dealt either with parts of our study area, or a single faulting type and coseismic slips only. The variability of the stress change calculations from friction coefficient, dip and rake angles were assessed following PARSONS (2005). The perspective of the stress field evolution calculations is the identification of active fault segments that are currently in stress enhanced areas; a first step for the seismic hazard assessment. We start with the stationary and conditional probability models estimation of the probability of occurrence in the next 30 years of an earthquake with $M \geq 6.5$ on known fault segments of the study area. Thereafter the accumulated stress changes due to coseismic slips of the modeled events were incorporated into the estimation of earthquake probability. Change in the probability on a given fault is calculated from the change in seismicity rate, which is computed taking into account both permanent and transient effects.

2. Seismotectonic Setting

The complexity of the plate interactions and associated crustal deformation in the eastern Mediterranean region is reflected in many destructive earthquakes that have occurred throughout its recorded history, and many of them are rather well documented and studied. The region features complex tectonics because it relates to the interaction of Eurasian, Arabian, and African lithospheric plates (Fig. 1). The subduction of the eastern Mediterranean oceanic lithosphere, the frontal part of the northward moving African lithosphere, along the Hellenic Arc is a key feature that influences the active deformation of the region, causing an extension of the continental crust in the overlying Aegean province (PAPAZACHOS and COMNINAKIS 1969, 1971; PAPAZACHOS *et al.*, 1998).

North and East Anatolian faults represent the lateral movement of Turkey toward the west (MCKENZIE, 1970). This motion is transferred into the Aegean in a southwesterly direction. It has been suggested that the Aegean Sea and much of Anatolia should be considered as two separate microplates observed from geodetic information combined with the seismological data (TAYMAZ *et al.*, 1991a; JACKSON, 1994; PAPAZACHOS, 1999; MCCLUSKY *et al.*, 2000; NYST and THATCHER, 2004). The southern boundary of the south Aegean plate is defined by low angle thrust faults that are located along the Hellenic Arc (PAPAZACHOS *et al.*, 1984, 1998; TAYMAZ, 1990, 1996). Interplay between dynamic effects of the relative motions of adjoining plates thus controls the

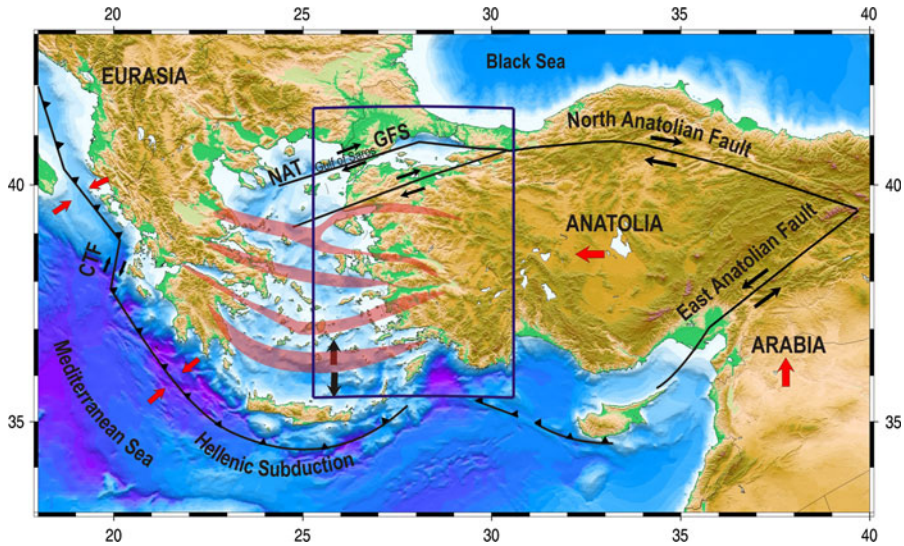

Figure 1
Summary sketch map of the active tectonic boundaries in the eastern Mediterranean Sea region. Large *arrows* show relative motions of plates with respect to Eurasia. The main extensional structures are shaded in *red*. *NAT* North Aegean Trough, *CTF* Cephalonia Transform Fault (after Papazachos *et al*., 1998; Armijo *et al*., 1999; McClusky *et al*., 2000)

large-scale crustal deformation and the associated earthquake activity in the study area.

Our study area is one of the most seismically active and deforming regions in the world bounded on the north by the NAF and the Ganos Fault System (GFS). The NAF is one of the longest active right lateral strike-slip fault systems, of about 1,500 km in length extending from eastern Turkey, through the Marmara Sea where it bifurcates into two branches. Along its northern branch, the Ganos Fault System constitutes the most significant tectonic element controlling the tectonic evolution of the area. The western termination of this fault system is in the Gulf of Saros, which is a neotectonic basin with ENE trending depression placed at the northeastern part of the Aegean Sea, where the North Aegean Trough (NAT) is developed. The dextral strike-slip motion of NAF is translated into the Aegean where it additionally accommodates the rapid N–S extension of the backarc Aegean region. Western Turkey is located in the boundary area between these regions and it has been under an N–S extension since Late Oligocene (Saunders *et al*., 1998). The major neotectonic features of western Turkey are the E–W trending grabens (e.g., Gediz, Küçük Menderes, Büyük Menderes) and their basin bounding active normal faults (Fig. 2) as well as other less prominent structures with NE–SW trending basins (e.g., Seyitoğlu and Scott, 1991; Taymaz and Price, 1992; Westaway, 1993; Bozkurt, 2001, 2003).

3. Methodology

The stress evolutionary model that is applied in the present study was proposed by Deng and Sykes (1997) and originally tested in southern California. Cumulative stress changes are assumed to arise from the following two sources: Tectonic loading generated by plate motions and coseismic displacements on faults associated with earthquakes. Interseismic stress accumulation between strong events is modeled by introducing "virtual negative displacements" along the major regional faults using the best available information on their long-term slip rates. These virtual dislocations are imposed on the faults with sense of slip opposite to the observed slip. The magnitude of this virtual slip is incremented in time according to the long-term rate of the fault. This is equivalent to the constant positive slip extending from the bottom of the seismogenic layer to infinite depth. Hence, tectonically-induced stress builds up in

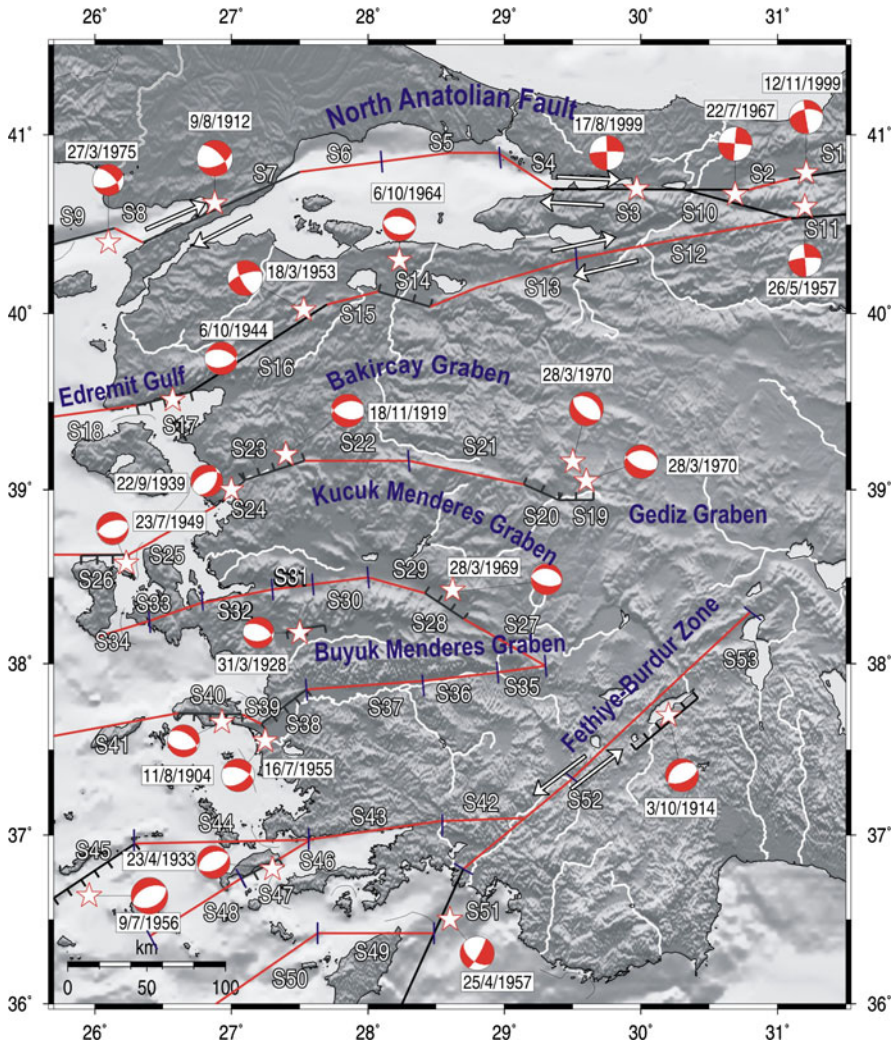

Figure 2
Simplified map of active faulting in the area of western Turkey. The code names of the fault segments are shown next to each segment. The segments that are associated with earthquakes of $M \geq 6.5$ that occurred since 1900, are shown in *black*. The fault plane solutions of $M \geq 6.5$ events are shown as lower hemisphere equal area projection whereas their epicenters are denoted by stars, linked with a light line with the beach balls. The occurrence day of each event (month/date, year) is given on top of the focal spheres

the vicinity of faults during interseismic periods. All computed interseismic stress accumulation is associated with the deformation caused by the time-dependent virtual displacement on major faults extending from the free surface to the seismogenic depth. Stress build-up is released wholly or in part during the next strong earthquake, with positive real displacements on given fault segments. Changes in stress associated with strong earthquakes are calculated for coseismic displacements on the ruptured fault segment and by adding the changes in the components of the stress tensor together as they occur in time.

Stress changes associated with both the virtual dislocations and actual earthquake displacements are calculated using a dislocation model of a planar fault surface, Σ, embedded in an elastic half space (Okada, 1992). Earthquakes occur when stress exceeds the strength of the fault. The closeness to the failure was quantified by using the change in Coulomb failure

function (ΔCFF). It depends on both changes in shear stress, $\Delta\tau$, and normal stress, $\Delta\sigma$, and in the presence of pore fluid it takes the form:

$$\Delta CFF = \Delta\tau + \mu(\Delta\sigma + \Delta p), \quad (1)$$

where $\Delta\tau$ is the shear–stress change (computed in the slip direction), $\Delta\sigma$ is the fault–normal stress change (positive for extension), Δp is the pore pressure change within the fault, and μ is the friction coefficient, which ranges between 0.6 and 0.8 (Harris, 1998 and references therein). Throughout this study we ignore the time-dependent changes in pore fluid pressure and consider only the undrained case (Beeler *et al.*, 2000), meaning that Δp depends on the fault–normal stress whereas the fluid mass content per unit volume remains constant. Induced changes in pore pressure resulting from a change in stress under undrained conditions, according to Rice and Cleary (1976) are calculated from:

$$\Delta p = -B\frac{\Delta\sigma_{kk}}{3}. \quad (2)$$

B is the Skempton's coefficient, where $0 \leq B < 1$, and $\Delta\sigma_{kk}$ indicates summation over the diagonal elements of the stress tensor. The Skempton's coefficient, B, denotes the relative proportion of fault–normal stress and change in pore pressure as it is assumed in Coulomb stress analysis (see King *et al.*, 1994; Harris, 1998, and references therein). If the air fills the pores then B is nearly zero, whereas if water fills the pores, it is typically between 0.5 and 1.0 for fluid-saturated rock and close to 1.0 for fluid-saturated soil. Sparse experimental determinations of B for rocks indicate a range from 0.5 to 0.9 for granites, sandstones, and marbles (Rice and Clearly, 1976). We assume a $B = 0.5$ and $\mu = 0.75$ (as in Robinson and McGinty, 2000; among others). If in the fault zone $\Delta\sigma_{11} = \Delta\sigma_{22} = \Delta\sigma_{33}$, so that $\Delta\sigma_{kk}/3 = \Delta\sigma$, then the apparent coefficient of friction is defined as $\mu' = \mu(1 - B)$. The above selected values for B and μ result to a value of apparent coefficient of friction equal to 0.4, which is widely used in studies of Coulomb stress modeling. We will investigate the effects of different values of Skempton's coefficient, B, namely equal to 0.2 and 0.9, which are the extreme values expressing the percentage of water filling the pores.

In Eq. 2 $\Delta\sigma_{kk}$ is the summation of the stress normal components, which, along with $\Delta\tau$ are calculated according to the fault plane solution of the next earthquake in the sequence of events, whose triggering is inspected. $\Delta\tau$ is positive for increasing shear stress in the direction of the relative slip on the observing fault while $\Delta\sigma$ is positive for tensional normal stress. When compressional normal stress on a fault plane decreases, the static friction across the fault plane also decreases. A positive value of ΔCFF for a particular fault denotes movement of that fault towards the failure (that is, likelihood that it will rupture in an earthquake is increased). The shear modulus and Poisson's ratio are fixed at 3.3×10^5 bar and 0.25, respectively.

Earthquakes nucleating on active fault surfaces are often approximated with rectangles dipping within the brittle layer of the Earth's crust. Fault planes are adequately described by the use of geometrical parameters such as the length, L, and the width, w, of the fault zone, and the fault plane solution. To calculate the rupture parameters that are necessary for the model application we use empirical relationships when field observations or relevant information from previous investigations are not available. These relationships are taken from Papazachos *et al.* (2004) who collected worldwide data and proposed scaling laws for different seismotectonic environments, according to which fault length, (L, in km), and coseismic displacement, (u, in cm), can be calculated as a function of the earthquake magnitude. For the dip slip faults the following scaling laws are derived:

$$\log L = 0.50M - 1.86, \quad (3)$$

$$\log u = 0.72M - 2.82, \quad (4)$$

whereas for strike-slip faults the respective equations are:

$$\log L = 0.59M - 2.30, \quad (5)$$

$$\log u = 0.68M - 2.59. \quad (6)$$

Estimates from Eqs. 3–6 and the respective relations proposed by Wells and Coppersmith (1994) were found to be in a good agreement.

When the seismic moment (M_o) of an earthquake is known the coseismic displacement, $\overline{u}$, is calculated from the following equation:

$$M_o = \mu \cdot \overline{u} \cdot S = \mu \cdot \overline{u} \cdot L \cdot w, \quad (7)$$

where μ is taken equal to 3.3×10^5 bar, as above, and S is the fault surface ($S = L\ w$). Fault width, in km, was estimated from the dip angle of the fault and the distance measured down-dip from the surface to the upper and lower edges of the rectangular dislocation plane, respectively.

For the evolutionary model application, it is necessary to define the seismogenic layer where the distribution of the coseismic slip is considered. In our study area it is known that the majority of the foci of the crustal earthquakes are located in the depth range of 3–15 km, which defines the brittle part of the crust. Considering all the above information combined with previous investigations for the study area (Papadimitriou and Sykes, 2001), the seismogenic layer in our calculations is taken to be in this range (3–15 km) for all the strong events ($M \geq 6.5$) modeled.

In addition to the fault geometry parameters, knowledge of the fault plane solutions is essential because the variation of these parameters affects the shape of the calculated stress field. Information on the events' fault plane solutions and moment magnitudes was collected from several studies (Global CMT solutions; McKenzie, 1972; Eyidoğan and Jackson, 1985; Eyidoğan, 1988; Taymaz *et al.*, 1991b; Taymaz and Price, 1992; Kiratzi and Louvari, 2001; Barka *et al.*, 2002; Papazachos and Papazachou, 2003). The fault planes are defined with the use of available field surveys, surface ruptures and in the absence of visible tectonic features of their corresponding faults, the ones consistent with the regional stress field are chosen. Magnitudes that are provided from Papazachos and Papazachou (2003) are equivalent moment magnitudes, M_w^* (Papazachos *et al.*, 1997).

4. Long-term Slip Rate Constraints on Major Faults

The incorporation of the tectonic loading in the evolutionary stress field calculations requires the identification of the position and geometry of the major faults in the study area, along with the definition of the long-term slip rates on them. It is possible to estimate the slip rates on the existing faults by using the relative motions between GPS stations straddling them. Such information is available mostly from Armijo *et al.* (2003) who decomposed the present-day GPS velocity into two superposed velocity fields, associated with corresponding sets of slip rates on the major structures, and Reilinger *et al.* (2006) who presented a new GPS-derived velocity field including data from 1988 to 2005, updating the results by McClusky *et al.* (2000; 2003). These observations deal with the zone of interaction of the Arabian, African (Nubian, Somalian) and Eurasian plates, adjacent parts of Zagros and central Iran, Turkey and the Aegean/Peloponnesus relative to Eurasia.

Active faults in western Turkey, Aegean and the Greek mainland, are closely related with the plate boundary processes, namely, the westward propagation of the North Anatolian Fault System and the Aegean extension related to subduction processes. GPS measurements have shown that large regions of the lithosphere move coherently while deformation is mostly localized on a small number of structures that extend to the base of the lithosphere. During the interseismic period, a fault is locked at seismogenic depths in the brittle schizosphere. In the lower part of the crust, in the plastosphere, the fault is continuously creeping, loading its locked upper part. Block boundaries have been determined from geologically active faults, which account for the present-day block motions and regional deformation, seismicity and historic earthquakes.

Armijo *et al.* (2003) incorporated both the geodetic and the geological constraints and provide a robust description of the present-day deformation of the Anatolian–Aegean region. They use for their model localized deformation zones, which are represented by dislocation elements and extended from the base of the lithosphere to the locking depth at the base of the seismogenic layer. Some representative values of slip rates on elements at the area of NAF are 12–20 mm/year at the northern strand of NAF, 12 or 2–6 mm/year at the southern part of NAF. Other recent GPS data indicate rates of about 15–25 mm/year (Reilinger *et al.*, 1997; McClusky *et al.*, 2000, 2003) or 24 ± 1 mm/year (Reilinger *et al.*, 2006).

The latter authors used a simple, kinematic block model, including elastic strain accumulations on the block-bounding faults, to quantify relative block motions and to determine present-day rates of the strain accumulation on the block bounding faults.

Normal faulting in the area of western Turkey is related with backarc extension of the Aegean. Stretching appears localized in a few regularly spaced rift zones in the Aegean which taper out into Anatolia and Greece (Flerit *et al*., 2004). These rift zones are flanked by active faults, some of them being associated with the strong events modelled in this study, or with historical events. The extension rates of these fault segments range between 2 and 6 mm/year for the central part of western Turkey, whereas at the southern part reach values up to 8 mm/year. The transtensional character for some of these faults up to the central western part is modelled by a strike-slip component of the order of 1–2 mm/year (Armijo *et al*., 2003; Reilinger *et al*., 2006).

The defined major active fault segments and their long-term slip rates with their code names are shown in Fig. 2 along with the fault plane solutions of the modeled strong events ($M \geq 6.5$), as lower-hemisphere equal-area projections. Information on the names of the fault segments, their code names, geographical position, geometry (strike and dip) and their average long-term slip rates is given in Table 1. All values of slip rates represent about 60% of the slip rates provided by Armijo *et al*. (2003), Flerit *et al*. (2004) and Reilinger *et al*. (2006) in order to account only for the seismically released strain energy. This constraint of the maximum possible accuracy slip rate for each fault segment will promote better estimates of earthquake hazard.

As regards the value of 60% of seismic coupling coefficient concerns, our choice was based on previous relevant investigations. According to Ambraseys and Jackson (1990) a significant proportion (as much as 60%) of the strain may be aseismic. Jackson *et al*. (1994) concluded that seismicity can account for at most 50% of the deformation in the Aegean area. King *et al*. (1994), comparing plate rates to seismic moment release rates at the area of California and Nevada, found that the relative plate motion occurred about 60% seismically and 40% aseismically. For the area of NAF in particular King *et al*. (2001) found that the rate of moment release accounts for about 60% of the relative plate motion. Davies *et al*. (1997) found that the seismic expression of strain for Greece accounts for only 20–50% of the geodetically determined strain. Ayhan *et al*. (2001) comparing GPS and seismic shear strain rates discovered that about 70% of GPS shear strain is accounted for by coseismic strain release. Bird and Kagan (2004) showed that continental transform faults (like NAF) have a 74% seismic coupling.

5. *Calculation of the Evolutionary Stress Field*

Stress changes, i.e., values of ΔCFF, are computed for the faulting types present in the study area, that is, right-lateral strike-slip faults oriented almost E–W or NE–SW and normal faults with almost E–W or ENE–WSW strike directions. At each stage of the evolutionary model, ΔCFF is calculated for a specific faulting type, that of the next inspected event. Information pertinent to the fault plane solutions of the events included in the calculations is given in Table 2 along with the rupture dimensions, length, L, and width, w, and the along strike, SS, and along dip direction, DS, coseismic slip, u, components.

Figures 3a–v are snapshots of ΔCFF at a depth of 10 km, chosen to be several kilometers above the locking depth (15 km) in the evolutionary model, since the nucleation depth is not known for most of the events. This is in agreement with King *et al*. (1994) who found that seismic slip peaks at mid-depths in the seismogenic zone. In these figures, blue regions denote negative changes in Coulomb stress models and are called stress shadows (Harris and Simpson, 1993, 1996). Yellow to red areas are characterized as stress bright zones, representing positive values of ΔCFF. Pure green area indicates no significant change in CFF. Shadow zones and bright zones are specific to the strike, dip and rake angles of the fault that experiences the ΔCFF. We will present that, in each stage of the stress evolution calculations, the strong events are located inside the stress enhanced areas. The same applies for moderate events with faulting similar to the type for which the stress calculations were performed.

Table 1

Information on the fault segments on which tectonic loading is considered for the evolutionary stress field calculations

Segment number	Code name	Fault segment start		Fault segment end		Strike (°)	Dip (°)	Length (km)	Width (km)	Faulting type	SS	DS
		Latitude °N	Longitude °E	Latitude °N	Longitude °E						mm/year	mm/year
S1	Duzce	40.75	31.08	40.83	31.73	262	53	56	0–19	RS	−7.2	0.0
S2	Karadere	40.69	30.79	40.75	31.08	255	55	26	0–18	RS	−7.2	0.0
S3	Izmit	40.70	29.35	40.69	30.79	268	84	120	0–15	RS	−10.8	0.6
S4	Cinarcik	40.70	29.35	40.90	28.95	308	88	40.4	0–15	RS	−10.2	4.8
S5	Marmaras 1	40.90	28.95	40.85	28.10	263	84	75	0–15	RS	−11.4	0.0
S6	Marmaras 2	40.85	28.10	40.79	27.50	263	78	51	0–16	RS	−11.4	0.0
S7	Ganos	40.40	26.35	40.79	27.50	68	55	110	0–18	RS	−12	0.6
S8	Saros 1	40.48	26.15	40.40	26.35	297	60	20	0–17	RS	−12	3.0
S9	Saros 2	40.39	25.70	40.48	26.15	68	55	40	0–18	RS	−12	3.0
S10	Mudurnu	40.53	31.10	40.70	30.30	275	88	80	0–15	RS	−3.6	1.8
S11	Abant	40.53	31.10	40.60	32.20	265	78	90	0–16	RS	−7.2	0.0
S12	Iznik	40.53	31.10	40.31	29.53	260	78	135.5	0–16	RS	−3	0.6
S13	Bursa 1	40.31	29.53	40.04	28.46	248	78	95.7	0–16	RS	−3	0.6
S14	Manyas	40.12	28.08	40.04	28.46	280	50	35	0–19	N	−0.6	3.0
S15	Yenice 1	40.05	27.70	40.12	28.08	256	70	33.2	0–16	RS	−1.2	0.0
S16	Yenice 2	40.05	27.70	39.56	26.70	250	70	101	0–16	RS	−1.8	0.0
S17	Edremit1	39.48	26.31	39.56	26.70	74	46	35	0–21	N	−1.2	2.4
S18	Edremit2	39.48	26.31	39.41	25.60	82	45	61.3	0–21	N	−1.2	2.4
S19	Gediz1	38.94	29.4	38.94	29.65	270	35	24	0–26	N	0.0	1.6
S20	Gediz2	39.03	29.14	38.94	29.40	308	35	24	0–26	N	0.0	1.6
S21	Bergama1	39.16	28.30	39.03	29.14	282	35	74	0–26	N	0.0	1.6
S22	Bergama2	39.16	27.54	39.16	28.30	271	35	66	0–26	N	−0.6	3.0
S23	Soma	39.05	27.10	39.16	27.54	253	45	43	0–21	N	−0.6	3.0
S24	Dikilli	39.05	27.10	38.90	26.88	211	45	26	0–21	N	−0.6	3.0
S25	Elaia	38.90	26.88	38.63	26.25	241	45	62.8	0–21	N	−1.2	1.8
S26	Chios	38.63	26.25	38.63	25.70	84	36	47.6	0–26	N	0.0	3.6
S27	Philadelphia	38.26	28.70	38.00	29.30	328	45	60.36	0–21	N	−0.6	2.4
S28	Alasehir	38.41	28.42	38.26	28.70	281	34	25	0–27	N	−0.6	2.4
S29	Sardeis	38.41	28.42	38.50	28.00	286	35	38	0–26	N	−0.6	2.4
S30	Turgutlu	38.50	28.00	38.46	27.60	263	45	35	0–21	N	0	3.6
S31	Kemalpasa	38.46	27.6	38.43	27.30	263	45	26	0–21	N	0	3.6
S32	Izmir	38.40	27.00	38.15	26.00	260	45	47	0–21	N	0	3.6
S33	Cezme	38.25	26.40	38.35	26.77	252	45	34	0–21	N	0	3.6
S34	Urla	38.35	26.77	38.43	27.30	252	45	37	0–21	N	0	3.6
S35	Denizli	37.85	27.55	37.95	28.95	83	45	31	0–21	N	−0.6	4.2
S36	Nazili	37.85	27.55	37.90	28.40	84	45	48	0–21	N	−0.6	4.2
S37	Aydin	37.90	28.40	37.95	28.95	86	45	75	0–21	N	−0.6	4.2
S38	Kusadaci 1	37.65	27.22	37.85	27.55	55	51	36	0–19	N	−0.6	4.2
S39	Kusadaci 2	37.71	27.08	37.65	27.22	117	45	16	0–21	N	0	0.6
S40	Samos	37.71	26.61	37.71	27.08	91	45	46	0–21	N	0	3.0
S41	Ikaria	37.71	26.61	37.58	25.70	80	45	80	0–21	N	0	2.4
S42	Mugla	37.08	28.53	37.10	29.14	88	45	54	0–21	N	0	3.0
S43	Marmaris	36.97	27.55	37.08	28.53	83	45	88	0–21	N	0	3.0
S44	Kalymnos	36.95	26.30	36.97	27.55	90	45	111	0–21	N	0	3.0
S45	Amorgos	36.41	25.30	36.95	26.30	65	40	100	0–23	N	0	2.4
S46	Bodrum	36.98	27.60	36.86	27.35	59	50	26	0–19	N	0	3.0
S47	Kos	36.74	27.07	36.86	27.35	65	50	28	0–19	N	0	3.0
S48	Astypalaia	36.74	27.07	36.40	26.40	58	50	71	0–19	N	0	3.0
S49	Symi	35.90	26.71	36.42	27.63	91	45	91	0–21	N	0	0.6
S50	Tilos	36.80	28.70	35.99	28.25	56	50	100	0–19	N	0	0.6
S51	Rodos	36.42	27.63	36.42	28.65	30	80	98	0–15	LS	0	1.8
S52	Fethiye	37.32	29.48	36.80	28.70	50	80	90	0–15	LS	0	1.8

Table 1 continued

Segment number	Code name	Fault segment start		Fault segment end		Strike (°)	Dip (°)	Length (km)	Width (km)	Faulting type	SS	DS
		Latitude °N	Longitude °E	Latitude °N	Longitude °E						mm/year	mm/year
S53	Burdur	38.30	30.80	37.32	29.48	50	80	158	0–15	LS	0	1.8

Some of these segments are associated with the strong ($M \geq 6.5$) modeled events or with known historical events. The first two columns give the number (as it appears in Fig. 2) and the code name of each fault segment. The next four columns give the geographical coordinates of the segment edges. The fifth and sixth columns give the strike and dip angles, respectively, for each segment, whereas the seventh and eighth columns give the corresponding fault length and width. The faulting type of each segment is indicated in the 11th column (*RS* right–lateral strike-slip; *N* normal; *LS* left–lateral strike-slip). The last two columns give the annual slip rate assigned in each segment (*SS* strike-slip component, negative for dextral motion; *DS* dip-slip component: positive for normal faulting)

The fault segment associated with the occurrence of each incoming earthquake is shown in Fig. 3 by a black color and the faults that already failed are in white, where the changes in stress are presented for the whole study area. In Fig. 3a, c–i, k–l, o, and q–s the calculations of ΔCFF were performed for normal or oblique normal faulting type. The remaining figures show the evolutionary stress field calculated for dextral strike-slip faulting. Initial values of ΔCFF are assumed to be zero everywhere on each fault plane just before the Samos earthquake of 1904, which is the first strong event in our data sample.

Figure 3a, displays the coseismic stress changes associated with the 1904 Samos event, which created a shadow zone for the normal faulting type. Bright zones are observed to the east and west. We expect these stress changes to affect the occurrence of future events. The 1912 Ganos earthquake occurred between the Gulf of Saros and the Sea of Marmara at the western part of the North Anatolian Fault. Figure 3b shows the state of stress before its occurrence with respect to the 1904 baseline. The event is inside an area of positive static stress changes due to the virtual model of stress accumulation. The 1914 Burdur earthquake is located inside at the borders of a region of positive ΔCFF (Fig. 3c). The 1919, Soma earthquake is located inside a bright zone (Fig. 3d), when the evolutionary stress field is calculated just before its occurrence and according to its fault plane solution. An extended shadow zone covers the areas to the north and south of the 1919 rupture, due to the coseismic stress changes of the 1904 and 1912 earthquakes. The stress evolutionary model successfully explains the location of the 1928 Torbali and the 1933 Kos events since the causative faults are inside bright zones (Fig. 3e, f, respectively). The epicenter and part of the causative fault of the 1939 Dikili event are located inside the stress enhanced area (Fig. 3g), partly created from the 1919 occurrence. The shadow zone at the north of the study area is eliminated over time as stress accumulates from 1939 to 1944, thus creating a bright zone inside which the 1944 Ayvacik event is located (Fig. 3h). Figure 3i depicts the stress state before the occurrence of the 1949 Chios earthquake, with respect to the 1904 baseline, which reveals that the rupture zone is located in a region of positive ΔCFF.

The state of ΔCFF before the 1953 Yenice earthquake is shown in Fig. 3j. The rupture is located in a region of positive ΔCFF, although, as we will show later, a part of the surface plane is inside positive stress changes. Figure 3k shows the accumulated Coulomb stress just before the 1955 Agathonisi earthquake calculated according to its fault plane solution. The causative fault is located inside a region of positive ΔCFF, to the east of the 1904 rupture, which probably hastened the 1955 occurrence. Figure 3l shows the state of stress before the 1956 Amorgos large event, with the associated fault seated in a stress enhanced area.

The fault of the 1957 Rhodos earthquake is located at the borders of stress bright zone and stress shadow (Fig. 3m). The stress field shown in Fig. 3n is the result of the accumulated stress changes (since 1904) calculated according to the fault plane solution of the 1957 Abant event. Its rupture zone was located inside a large region of positive ΔCFF. We note here the positive effect of the large 1944 Bolu–Gerede

Table 2

Rupture models for earthquakes with $M \geq 6.5$ that occurred in the study area since the beginning of the twentieth century

Origin time epicenter					M_w^*	M_o ($\times 10^{26}$ dym cm)	Fault plane solution			L (km)	w (km)	SS (m)	DS (m)
Year	Date	Time	Latitude (°N)	Longitude (°E)			Strike (°)	Dip (°)	Rake (°)				
1904	Aug. 11	06:08:30	37.66	26.93	6.8 (4)		91	45	−115	46	17	−0.50	1.08
1912	Aug. 9	01:29:00	40.62	26.88	7.4 (2)	6.0 (2)	68	55	−145 (2)	110	14.6	−1.02	0.72
1914	Oct. 3	22:07:00	37.70	30.20	7.0 (5)	4.4 (4)	230	35	−105	52	21	−0.43	1.60
1919	Nov 18	21:54:50	39.20	27.40	6.9 (2)	1.38 (2)	253	45	−115 (2)	43	17	−0.26	0.57
1928	Mar. 31	00:29:47	38.18	27.50	6.5 (4)		83	45	−94	25	17	−0.05	0.72
1933	Apr. 23	05:57:37	36.80	27.30	6.6 (4)		65	50	−90 (6)	28	15.6	0.18	0.84
1939	Sep. 22	00:36:32	39.00	27.00	6.6 (4)		211	45	−115	26	17	−0.36	0.78
1944	Oct. 6	02:34:41	39.51	26.57	6.8 (2)		74	46	−114 (2)	35	17	0.41	1.12
1949	July 23	15:03:30	38.58	26.23	6.7 (4)	1.85 (6)	84	36	−80	31	20.4	0.17	1.01
1953	Mar. 18	19:06:16	40.02	27.53	7.2 (2)	8.7 (5)	250	70	−160	60	13	−3.55	1.29
1955	July 16	07:07:10	37.55	27.15	6.9 (4)		55	51	−133 (8)	38	15.4	−0.81	0.87
1956	July 9	03:11:40	36.30	25.70	7.7 (4)		65	40	−90 (9)	75	18.7	0.00	5.30
1957	Apr. 25	02:25:42	36.50	28.60	7.2 (5)	4.4 (5)	30	80	−41	67	12.2	1.01	0.88
1957	May 26	06:33:30	40.60	31.00 (1)	7.0 (2)	6.76 (2)	265	78	179 (2)	40	12.2	−1.47	−0.03
1964	Oct. 6	14:31:23	40.30	28.23 (2)	6.9		280	50	−90 (2)	35	16.7	−0.12	1.41
1967	July 22	16:56:58	40.67	30.69 (2)	7.2		275	88	−178 (2)	80	12	−2.02	0.07
1969	Mar. 28	01:48:29	38.42	28.6 (3)	6.5 (3)	0.625 (3)	313	34	−90 (3)	25	21	0.00	0.61
1970	Mar. 28	21:02:23	39.055	29.60 (3)	7.1 (3)	1.09 (3)	308	35	−90 (3)	24	21	0.00	1.60
1970	Mar. 28	23:00:00	39.16	29.50 (3)	7.1 (3)	3.06 (3)	270	35	−110 (3)	24	21	−0.82	2.25
1975	Mar. 27	05:15:08	40.40	26.10	6.6 (7)	0.64 (7)	68	55	−145 (2)	40	14.7	−0.70	0.49
1999	Aug. 17	00:01:37	40.76	29.97	7.4 (10)	1.31 (10)	268	84	180 (10)	35	12	−2.76	0.00
							260	87	164 (10)	20	12	−1.92	−0.55
							265	87	164 (10)	26	12	−3.36	−0.96
							271	87	164 (10)	35	12	−1.83	−0.52
1999	Nov. 12	20:00:00	40.79	31.21	7.2 (7)	6.56 (7)	262	53	−177 (11)	56	15	−2.06	−0.14

First five columns give information on the occurrence time and the epicentral coordinates of each event. The next two columns give the magnitude and seismic moment when available. The eighth through tenth columns give the strike, dip and rake angles of the fault plane. Eleventh and 12th columns give the fault length, L, and width, w. SS and DS in the last two columns, respectively, give the strike-slip component (negative for dextral faulting) and the dip-slip component (positive for normal faulting). Note that for the 1999 Izmit main shock a multi segmented fault is considered. Numbers in parentheses indicate references

References: 1. Ambraseys (2001); 2. Taymaz *et al.* (1991b); 3. Eyidoğan and Jackson, 1985; 4. Papazachos and Papazachou (2003); 5. Pacheco and Sykes (1992); 6. Eyidoğan, 1988; 7. Global CMT determination; 8. McKenzie (1972); 9. Shirokova (1972); 10. Barka *et al.* (2002); 11. Kiratzi and Louvari (2001)

earthquake (M 7.3), which occurred outside and to the east of our study area, as being along strike, created a wide stress enhanced zone encompassing the ruptures of 1957, 1967 and the two 1999 events (Nalbant *et al.*, 1998). In Fig. 3o the accumulated Coulomb stress changes just before the 1964 Manyas earthquake of 1964 are shown for faulting in agreement with its focal mechanism. The activated fault is situated in a stress-enhanced area. Figure 3p shows the accumulated stress changes calculated according to the fault plane solution and just before the occurrence of the 1967 Mudurnu earthquake which is probably inhibited by the 1957 Abant earthquake by the stress transfer between the two adjacent fault segments. Figure 3q shows the accumulated Coulomb stress changes just before the occurrence of the 1969 Alaşehir rupture, which is located in a stress enhanced area.

Figures 3r and s show the accumulated Coulomb stress just before the 1970 Gediz main shock and its major aftershocks, respectively. The activated faults are located inside stress-enhanced areas. The later one, occurring just 2 h after the first event, is most probably triggered by the first. Figure 3t shows the accumulated Coulomb stress changes just before the 1975 Saros event, occurring on a site where the 1912

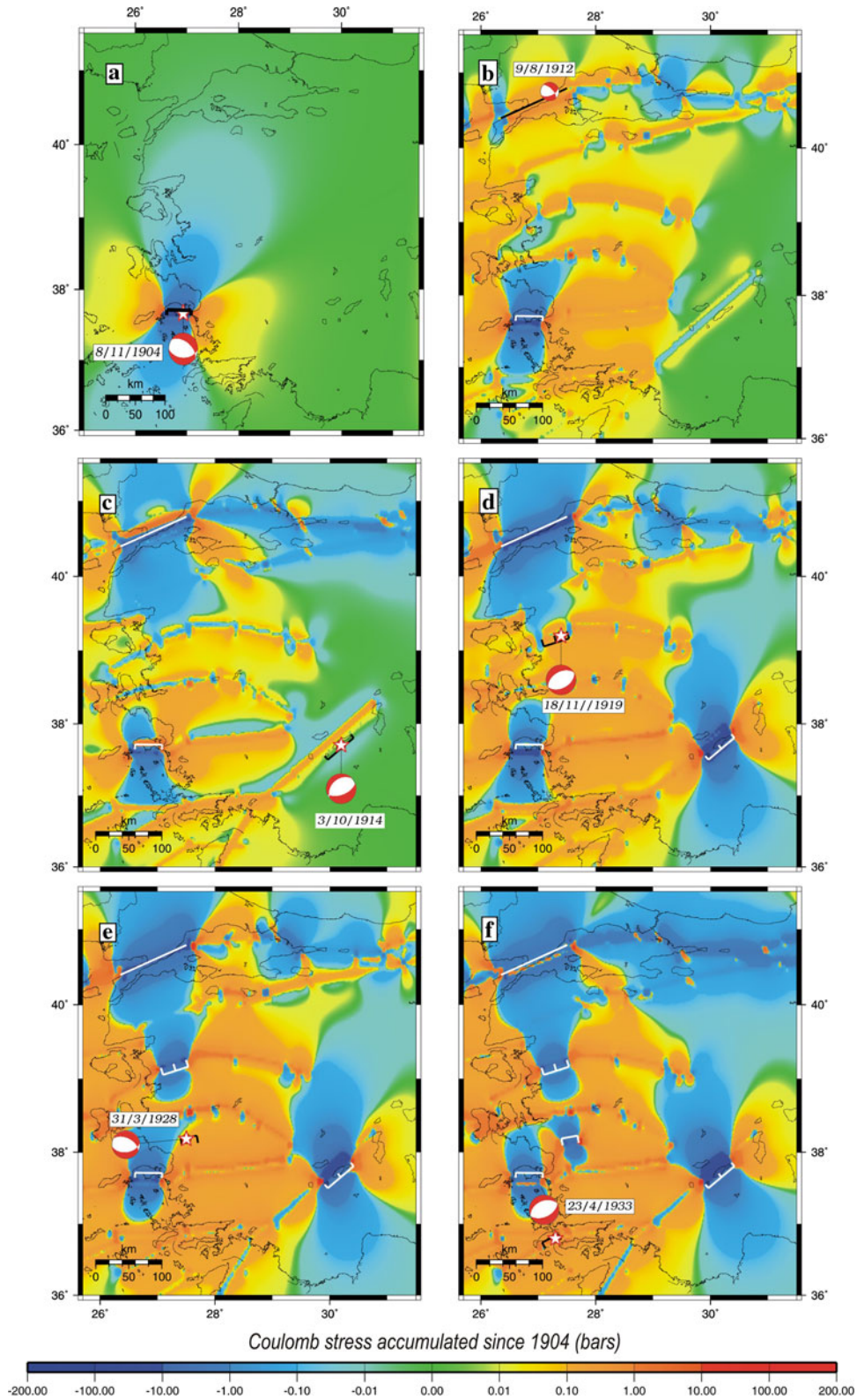
a
8/11/1904
b
9/8/1912
c
3/10/1914
d
18/11//1919
e
31/3/1928
f
23/4/1933
km
0 50 100
26° 28° 30°
40° 38° 36°
Coulomb stress accumulated since 1904 (bars)
-200.00 -100.00 -10.00 -1.00 -0.10 -0.01 0.00 0.01 0.10 1.00 10.00 100.00 200.00

Figure 3
Stress evolution in western Turkey and eastern Aegean Sea since 1904. Coulomb stress is calculated for dextral strike-slip and normal faults at a depth of 10 km. The stress pattern is calculated for the faulting type of the next strong event in the sample. The colour scale in the bottom shows the stress changes in *bars*. Fault plane solutions are denoted as in Fig. 2. Stars denote epicenters of earthquakes linked with a thin line with the beach balls. The fault segment associated with the occurrence of each event is shown by *black color*, while the segments that already failed are shown in white. **a** Coseismic Coulomb stress changes associated with the 1904 event. **b** Stress evolution until just before the 1912 Ganos event. Coseismic stress changes associated with the 1904 earthquake and tectonic loading on the fault segments since then are included. **c** State of stress before the 1914 Burdur earthquake. **d** ΔCFF before the 1919 Soma event. **e** State of stress just before the 1928 Torbali event. **f** Stress evolution before of the occurrence of the 1933 Kos event. **g** Coulomb stress changes before the 1939 Dikili earthquake. **h** Stress evolution until the 1944 Ayvacik main shock. **i** State of stress just before the 1949 Chios island event. **j** ΔCFF up to the 1953 Yenice earthquake. **k** Stress evolution before the 1955 Agathonisi earthquake. **l** State of stress just before the 1956 Amorgos main event. **m** Coulomb stress changes until the 1957 Rhodes earthquake. **n** Stress evolution just until the 1957 Abant earthquake. **o** State of stress before the 1964 Manyas earthquake. **p** Stress evolution until just before the 1967 Mudurnu earthquake. **q** ΔCFF just before the 1969 earthquake in Alaşehir. **r** State of stress before the first 1970 Gediz event, and **s** before the second 1970 Gediz event. **t** State of stress before the 1975 earthquake in Saros. **u** ΔCFF before the 1999 Izmit earthquake. **v** ΔCFF before the 1999 Düzce earthquake

Ganos earthquake has accumulated positive Coulomb stress changes. Figure 3u shows the accumulated stress changes calculated just before the occurrence of the 1999 Izmit (Kocaeli) large main shock, which is here shown as one fault segment, although a multi-segmented source is considered for its modeling. After the 1967 earthquake a bright zone had been created in this part of NAF; a branch of which includes the rupture zone of the 1999 event. An extended bright zone appeared at the eastern area of Kocaeli where the next Düzce earthquake occurred (Fig. 3v). This is in agreement with Parsons *et al.* (2000), Hubert-Ferrari *et al.* (2000) and Papadimitriou *et al.* (2001) who found that the spatial distribution of Coulomb Stress changes caused by the Izmit (Kocaeli) earthquake showed an extended stress enhanced zone comprising the rupture area of the Düzce earthquake. The bright zone in Fig. 3v that now encompasses the fault associated with the 1999 Düzce earthquake is evidently due to the stress changes caused by the Izmit coseismic slip, thus evidencing its possible triggering by the previous strong event.

We extended our calculations of the evolutionary stress field to 2008, whereas after 1999 no strong event ($M \geq 6.5$) has occurred in our study area. Figure 4 depicts the evolved stress state from 1904 to the present and includes the addition of coseismic stress changes associated with the occurrence of the 1999 Düzce earthquake and the stress accumulation caused by 105 years of tectonic loading. The stress field is inverted for three faulting types (dextral strike-slip, normal and sinistral strike-slip) and different values of the Skempton's coefficient ($B = 0.2$, $B = 0.5$ and $B = 0.9$), for testing the effect of the pore fluid on the stress changes calculations. The lower and maximum values assigned here are the extreme values that this coefficient can take, expressing the lower and maximum filling of the pores, respectively. Figures 4a–c shows the evolved stress change for a typical normal slip fault for the area (strike = 275°, dip = 45°, rake = −90°) along with the focal mechanisms of smaller magnitudes ($M < 6.5$) earthquakes since 1999. The same holds for Fig. 4d–f but for dextral strike-slip faulting (strike = 90°, dip = 87°, rake = −178°) and Fig. 4g–i for left-lateral strike-slip faulting (strike = 30°, dip = 80°, rake = −41°). Information regarding the fault plane solutions depicted in Fig. 4 is given in Table 3. A lower value of Skempton's coefficient ($B = 0.2$) is used in Fig. 4a, d and g where the stress pattern looks very similar to that depicted in Figs. 4b and 5b, which was calculated for $B = 0.5$. Figure 4c, f and i show the stress pattern calculated for a higher Skempton's coefficient ($B = 0.9$), in which the resulting pattern also remains almost unaffected. This shows that the value of the Skempton's coefficient selected ($B = 0.5$) is suitable for our calculations. Most of the smaller events plotted in Fig. 4 are located inside bright zones or in the borders between bright and shadow zones.

In order to investigate the effect of the evolutionary stress field on the incoming ruptures, the cumulative stress changes were calculated onto the rupture plane of each event just before its occurrence and are shown in Fig. 5. Although precise hypocenter location or details on rupture initiation are not available for the majority of the modeled events, and

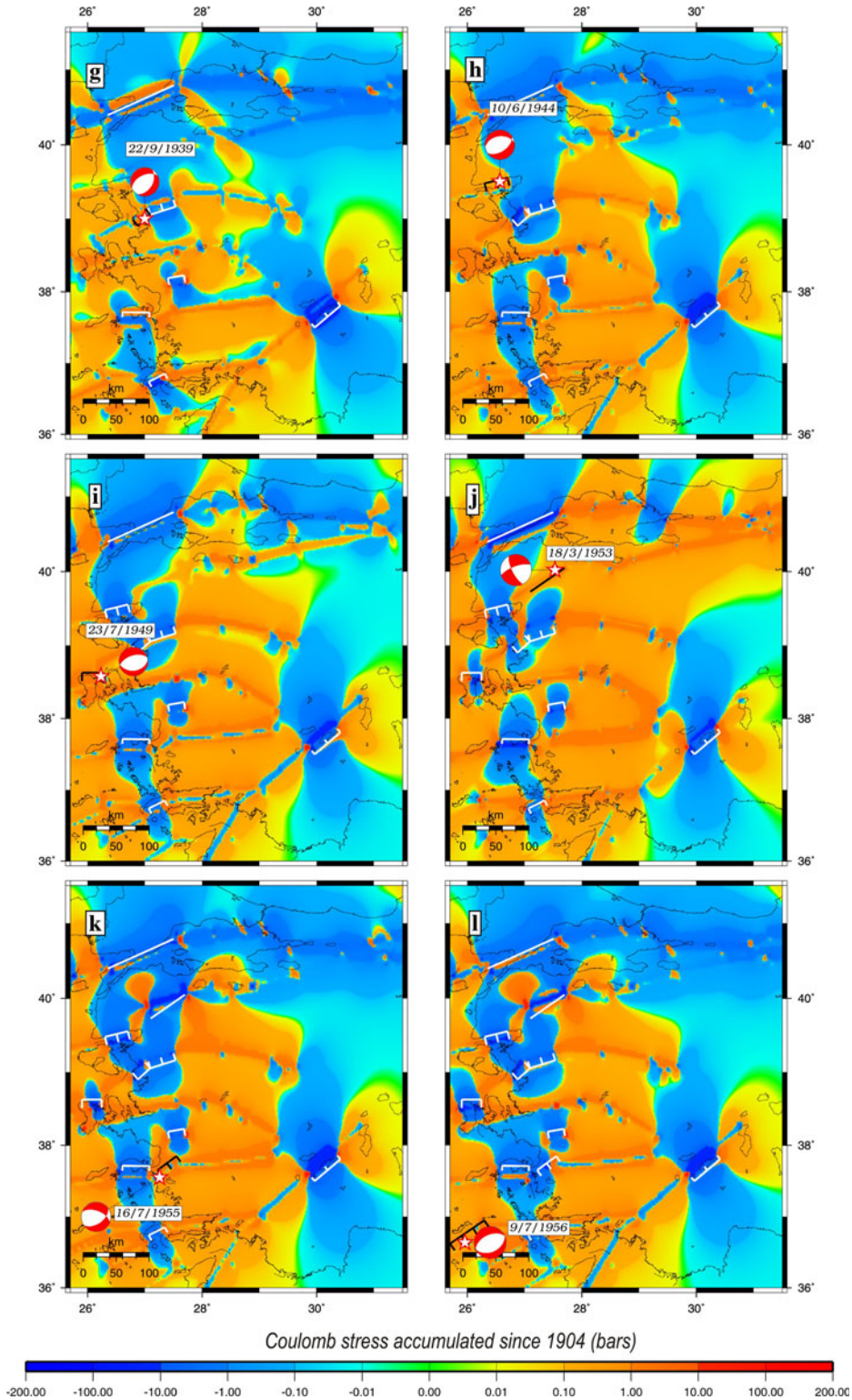

Figure 3
continued

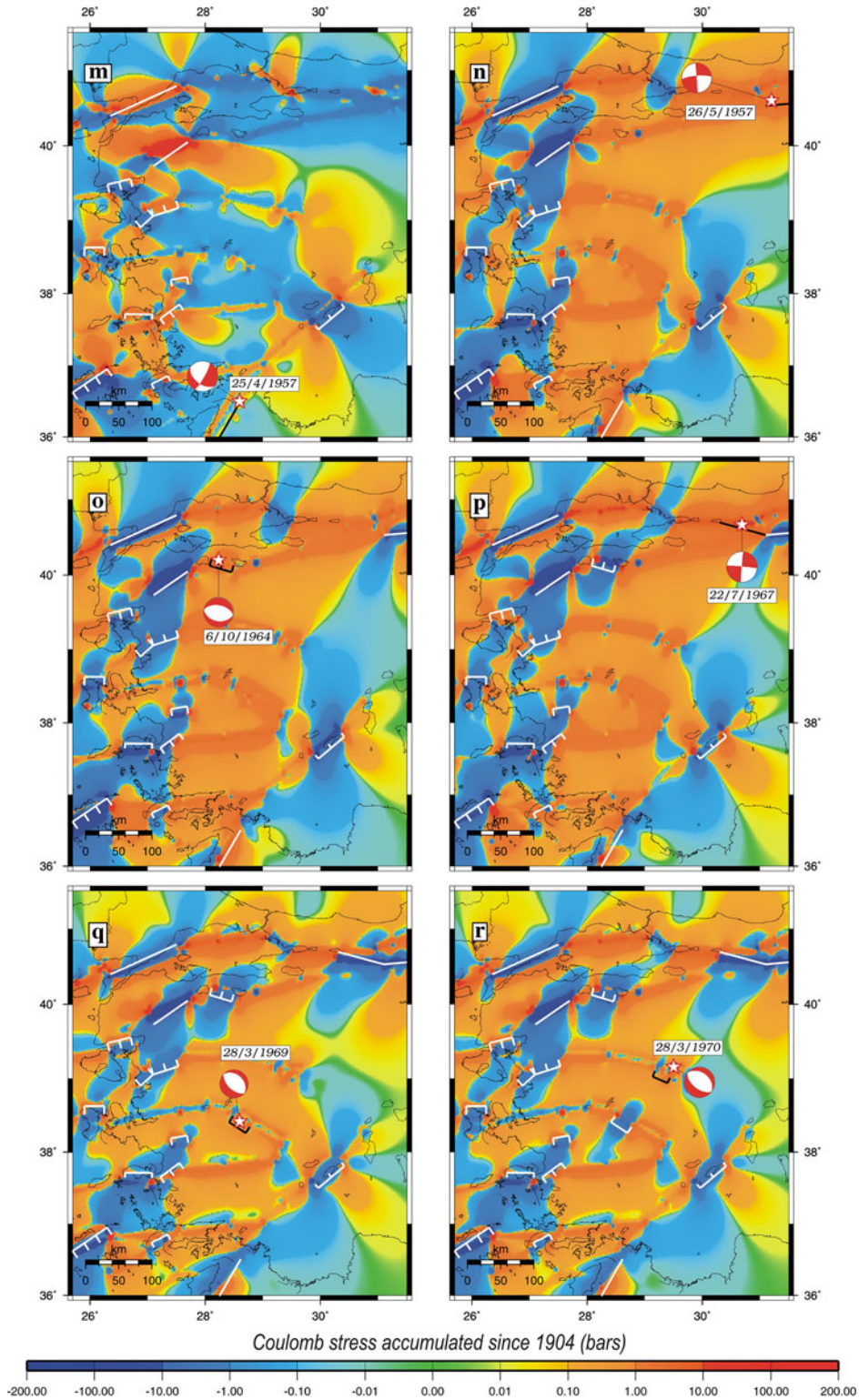

Figure 3
continued

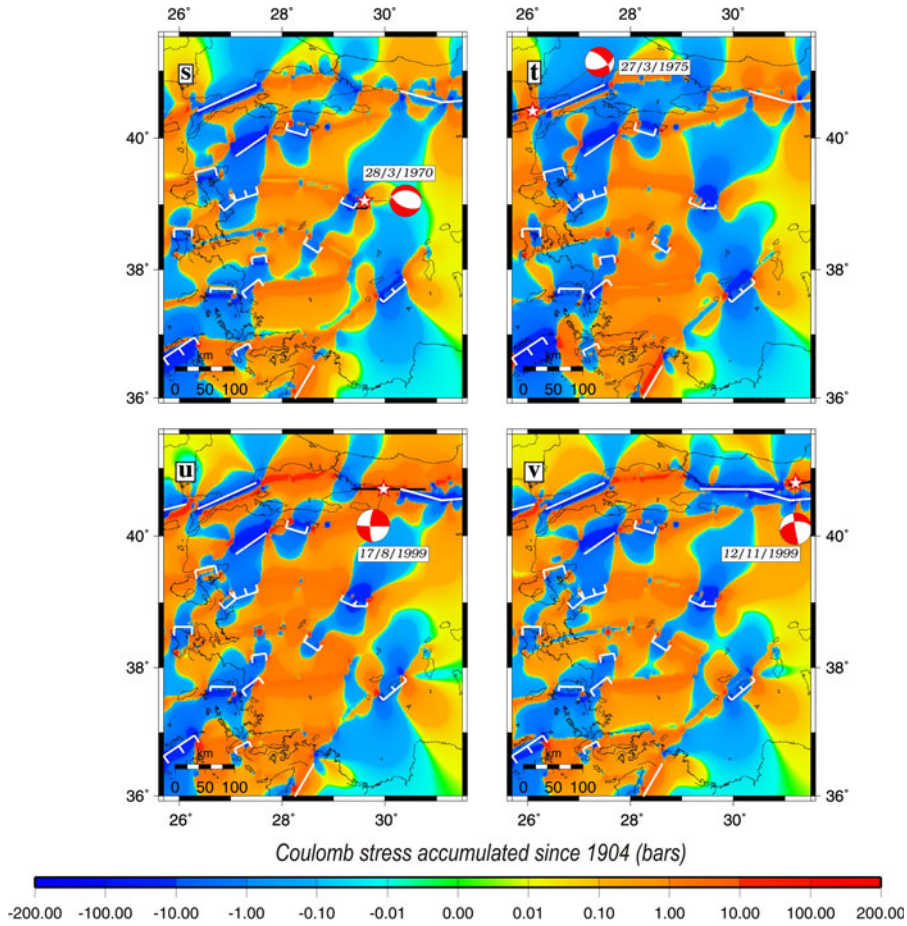

Figure 3
continued

in this case it is not feasible to correlate them with the position of the maximum ΔCFF, it is evident that in most cases the assumed rupture surfaces are inside stress enhanced areas. Examining the rupture plane of the normal faulting 1914 Burdur event (Fig. 5b), although it is influenced by tectonic loading on the nearby strike-slip Fetiye–Burdur fault, its occurrence is not inhibited since it is partially enhanced by positive stress changes. Even the rupture plane of the 1953 Yenice main shock, which is of strike-slip faulting in a parallel branch with the one associated with the 1912 Ganos event, is partially inhibited by this previous occurrence (Fig. 5i). It is thus worthy of note here, that the evolutionary model is adequate to explain the sequential occurrence of the strong events.

A quantitative evaluation of the calculation is given in Table 4, where the percentage of the rupture plane with positive or even larger of 0.1 bars, stress changes values is given (4th and 5th columns of the Table). Given the uncertainty in knowing the nucleation depth, this percentage is also estimated at depths of 6, 8, 10 and 12 km (last four columns of the Table), which are considered the most presumable depths for crustal events in the study area.

6. *Influence of the Skempton's Coefficient, and Rake and Dip Angles on the ΔCFF Calculations*

In order to investigate to which extend the uncertainties involved in the fault parameters (dip

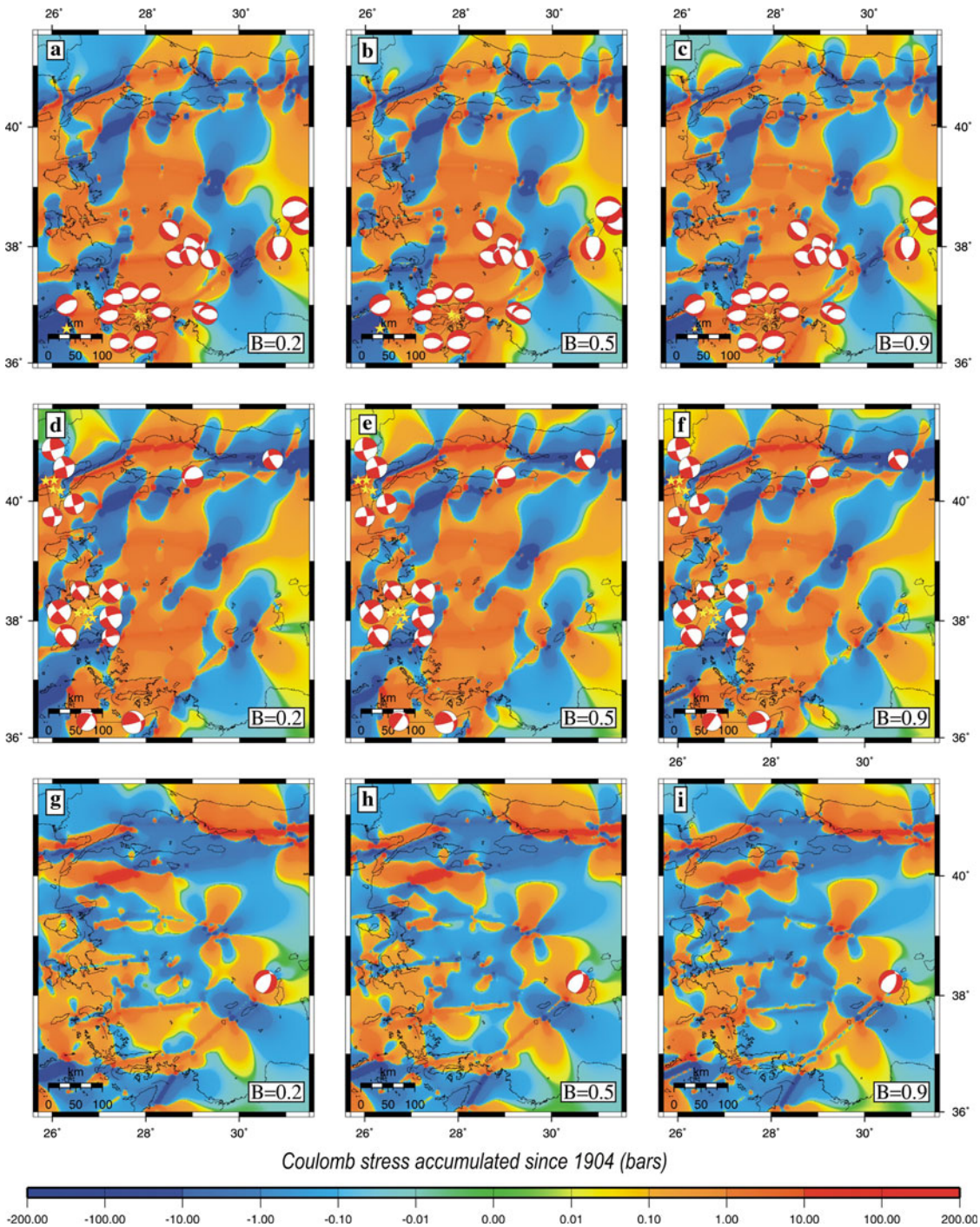

Figure 4

a Coulomb stress evolution until 2008 calculated for normal faulting representative (strike = 275°, dip = 45°, rake = 90°) of the area at a depth of 10.0 km for Skempton's coefficient equal to 0.2. The fault plane solutions of the events with $M \leq 6.5$ that occurred during 2000–2008 and are associated with normal faulting are also shown as lower-hemisphere equal area projections. **b** Same as **a** with $B = 0.5$. **c** Same as **a** with $B = 0.9$. **d** Same as in **a** but for dextral strike-slip faulting representative for the area (strike = 90°, dip = 87°, rake = 178°). **e** Same as in **d** but for $B = 0.5$. **f** Same as in **d** but for $B = 0.9$. **g** Same as in **a** but for sinistral strike slip faulting representative (strike = 30°, dip = 80°, rake = −41°) of the area. **h** Same as in **g** but for $B = 0.5$. **i** Same as in **g** but for $B = 0.9$

Table 3

Information on the available fault plane solutions for earthquakes that occurred in the study area from 1999 to present (Global-CMT determination)

Origin time		Epicenter		*M*	Depth (km)	Focal mechanism		
Year	Date	Longitude (°E)	Latitude (°N)			Strike (°)	Dip (°)	Rake (°)
2000	21 Apr.	29.39	37.78	5.4	15.0	110	23	−139
2000	23 Aug.	30.72	40.68	5.3	15.3	253	57	−160
2000	15 Dec.	31.35	38.40	6.0	15.0	285	41	−100
2002	3 Feb.	31.21	38.62	6.4	15.0	269	37	−71
2002	3 Feb.	30.56	38.23	5.8	15.0	236	45	−58
2002	3 Feb.	31.22	38.52	5.3	15.0	76	43	−70
2003	4 Oct.	26.86	38.05	5.7	15.0	155	70	−15
2003	17 Apr.	26.75	37.92	5.2	15.0	156	50	−15
2003	6 July	26.02	40.19	5.7	15.0	169	771	7
2003	6 July	26.17	40.17	5.2	15.0	73	77	173
2003	9 July	25.86	40.33	4.8	18.0	356	71	3
2003	23 July	28.77	37.88	5.3	15.0	97	31	−111
2003	26 July	29.05	38.03	5.4	15.0	60	57	−147
2004	15 June	26.04	40.34	5.2	12.0	342	78	5
2004	3 Aug.	27.93	36.77	5.2	12.0	74	38	−97
2004	4 Aug.	27.88	36.80	5.5	12.0	75	40	−95
2004	4 Aug.	27.97	36.82	5.2	12.0	71	42	−111
2004	4 Aug.	27.91	36.81	5.3	12.0	75	41	−94
2004	20 Dec.	28.33	36.88	5.3	12.0	105	45	−69
2005	10 Jan.	27.87	36.84	5.4	15.1	110	45	−63
2005	11 Jan	27.84	36.84	5.0	12.2	100	33	−69
2005	17 Oct.	26.82	38.15	5.5	15.2	242	61	−166
2005	17 Oct	26.62	38.18	5.8	12.0	231	76	−177
2005	17 Oct	26.54	38.12	5.2	17.8	250	42	−161
2005	20 Oct.	26.72	38.16	5.8	12.9	231	73	−169
2006	5 June.	28.65	37.80	4.8	21.7	295	34	−88
2006	24 Oct.	29.00	40.40	5.0	14.3	205	32	−144
2007	23 Jan.	28.52	38.28	4.9	13.2	301	28	−103
2007	30 Mar.	30.91	37.92	4.5	13.5	158	45	−129
2007	10 Apr.	30.87	37.96	5.1	14.6	161	50	−122
2007	31 Aug.	26.32	36.59	5.2	15.7	71	25	−83
2007	29 Oct.	29.21	36.89	5.3	12.0	275	37	−107
2007	16 Nov.	29.34	36.83	5.1	13.0	263	38	−108
2008	25 Apr.	28.94	37.84	5.0	12.2	276	28	−151

and rake angles) influence the calculated stress pattern, two earthquakes were selected and the correlation between calculated stress changes and different values of Skempton's coefficient, rake and dip angle of the fault are tested following the technique of Parsons (2005). We have chosen for this purpose a dip-slip and a dextral strike-slip event for the sake of comparison, and performed the calculations at a depth of 10 km.

The values of static stress changes at the hypocenter of the 1969 Alaşehir normal faulting earthquake ($M_w = 6.5$) as a function of assumed different values of the Skempton's coefficient ($0.2 \leq B \leq 0.9$) and varying the rake angles (ranging between $-70°$ and $-110°$ to keep the normal character of faulting) are shown in Fig. 6a. For a constant value of the rake angle variation, the selection of the Skempton's coefficient value, *B*, can cause differences in the calculated static stresses up to 0.2 bar (20% variation). Almost the same difference is found (0.16 bar) for dip angle variation when the calculations are performed for a constant value of *B* (12–13% variation). Keeping the rake value constant and equal to $-90°$, different dip angle values ranging from 30° to 60° were tested (considering that the typical mean value for crustal normal faults is 45°

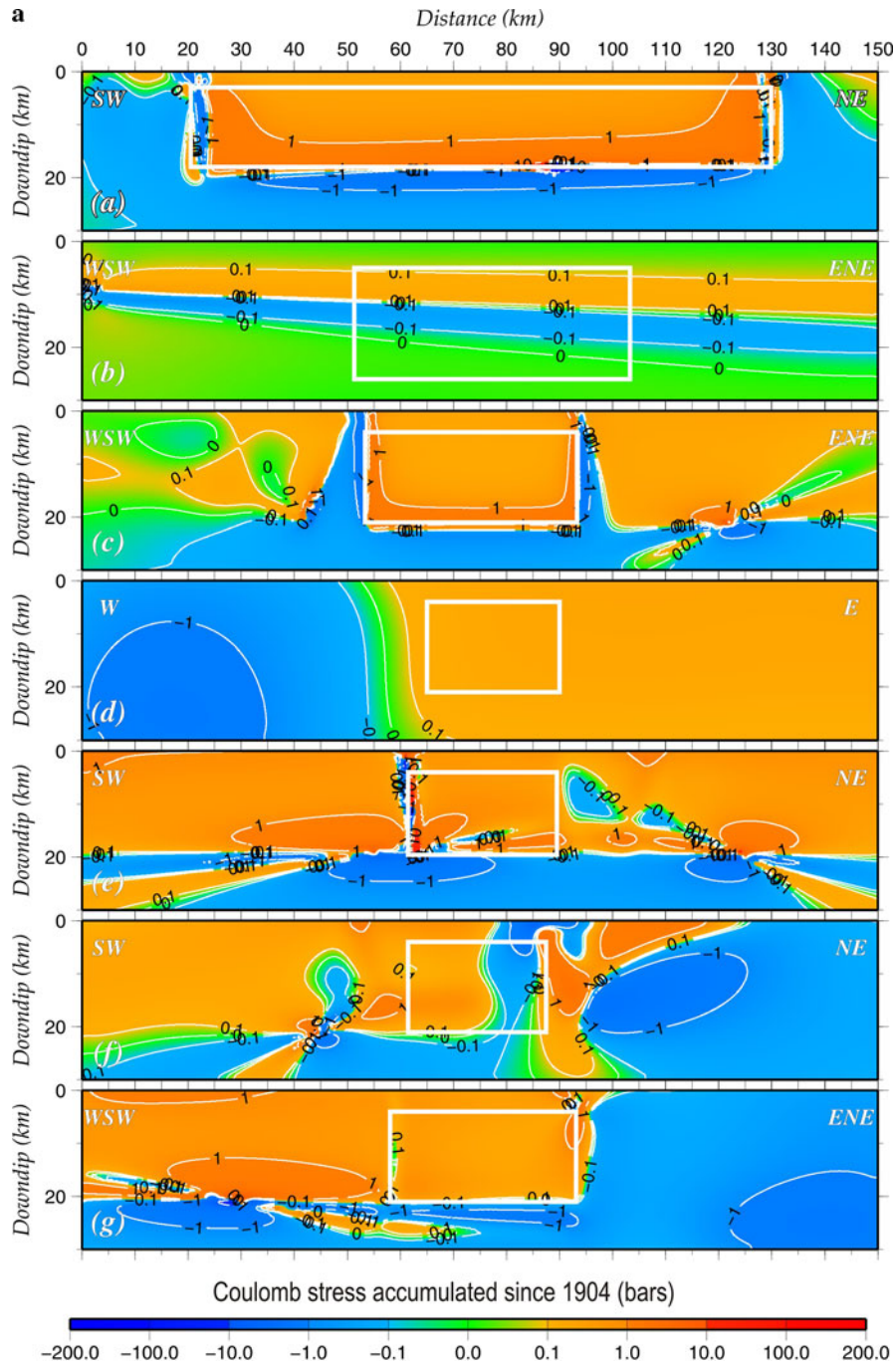

Figure 5

Accumulated static stress changes associated with the tectonic loading on the major faults and the coseismic slip of the earthquakes taken into account in the stress evolutionary model, resolved onto the rupture plane of the next strong event. *Contour lines* are accompanied with corresponding values of stress changes in *bars*. *Rectangles* denote the rupture areas, considered as rectangular surfaces with two edges parallel to the Earth's surface, for: **a** the 1912 Ganos main shock, **b** the 1914 Burdur earthquake, **c** the 1919 Soma main event, **d** the 1928 Torbali main shock, **e** the 1933 Kos earthquake, **f** the 1939 Dikili earthquake, **g** the 1944 Ayvacik event, **h** the 1949 Chios main shock, **i** the 1953 Yenice earthquake, **j** the 1955 Agathonisi event, **k** the 1956 Amorgos main shock, **l** the 1957 Rhodes earthquake, **m** the 1957 Abant earthquake, **n** the 1964 Manyas event, **o** the 1967 Mudurnu main shock, **p** the 1969 Alasehir earthquake, **q** the 1970 first Gediz event, **r** the 1970 second Gediz event, **s** the 1975 Saros main shock, **t** the 1999 Izmit main shock and **u** the 1999 Düzce event

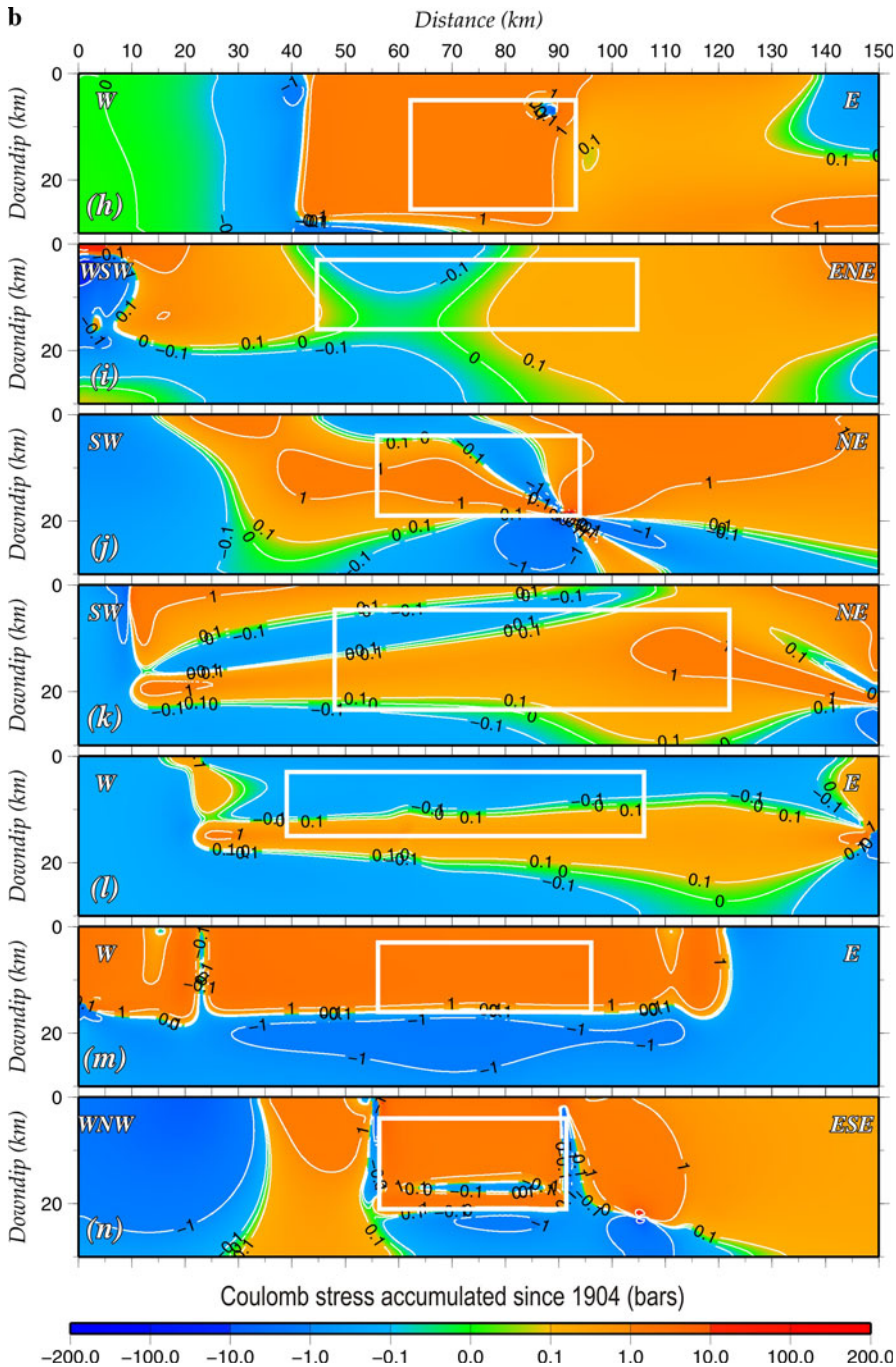

Figure 5
continued

and that the 1969 earthquake occurred on a fault with dip angle 34°, see Table 2). The stress changes were found to vary up to 0.7 bar (38–60% variation), whereas a change of up to 0.2 (11–12% variation) bar was found to depend on the variation of friction coefficient (Fig. 6b).

The same procedure was followed for the 1999 Düzce earthquake ($M_w = 7.2$) of dextral strike-slip

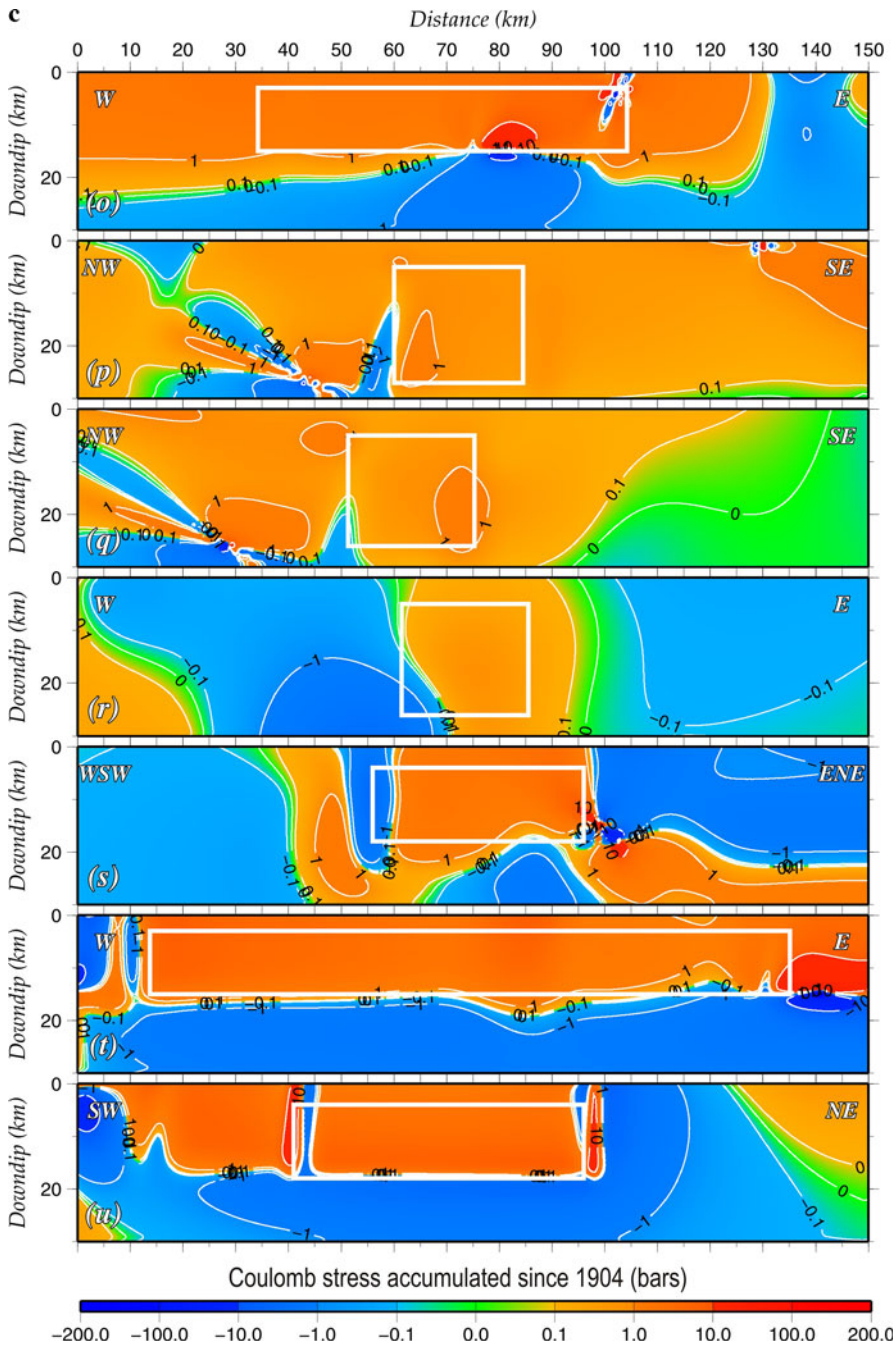

Figure 5
continued

faulting. We selected this event, which also has been tested by Parsons (2005), for the reasons stated by the above author and for the sake of comparison. The values of Skempton's coefficient are varied from 0.2 to 0.9 and the ones of the rake angle from −140° to −180° keeping the sense of the dextral strike slip faulting. Differences reaching 0.55 bar were found (5% variation) in the static stress changes depending on Skempton's coefficient, whereas these changes reached up to 1.5 bar (12–13% variation) for the rake

Table 4

Coulomb stress change values calculated onto the rupture planes of the modelled strong events

Occurrence Year	ΔCFFminimum (bars)	ΔCFF maximum (bars)	ΔCFF mean (bars)	Percentage $\Delta CFF > 0.0$ bars	Percentage $\Delta CFF > 0.1$ bars	Percentage $\Delta CFF > 0.1$ h = 6 km	Percentage $\Delta CFF > 0.1$ h = 8 km	Percentage $\Delta CFF > 0.1$ h = 10 km	Percentage $\Delta CFF > 0.1$ h = 12 km
1912	−256.25	95.96	0.92	94.78	94.67	96.33	97.25	97.25	97.25
1914	−0.50	0.28	−0.01	62.59	26.05	100.00	0.00	0.00	0.00
1919	0.26	3.17	0.75	100.00	100.00	100.00	100.00	100.00	100.00
1928	0.15	0.36	0.27	100.00	100.00	100.00	100.00	100.00	100.00
1933	−35.49	48.93	1.20	93.08	91.07	100.00	100.00	96.43	71.43
1939	−1.90	3.02	0.15	66.24	56.41	53.85	57.69	65.38	69.23
1944	−0.29	2.03	0.47	95.40	93.65	97.14	97.14	97.14	100.00
1949	−11.10	5.47	1.21	99.08	99.08	100.00	100.00	100.00	100.00
1953	−0.26	0.22	0.05	60.71	42.26	38.33	43.33	45.00	48.33
1955	−3.11	47.36	0.74	73.36	70.07	63.16	71.05	78.95	86.84
1956	−0.42	1.36	0.40	80.65	74.32	54.05	83.78	100.00	100.00
1957a	−0.58	1.16	−0.02	38.81	32.49	0.00	0.00	1.49	85.07
1957b	−0.32	3.21	2.23	94.82	93.93	100.00	100.00	100.00	100.00
1964	−4.33	6.41	1.72	92.38	91.43	97.14	97.14	97.14	22.86
1967	−92.47	44.56	3.73	97.47	97.36	97.14	97.14	98.57	100.00
1969	0.11	1.20	0.85	100.00	100.00	100.00	100.00	100.00	100.00
1970a	−0.13	1.29	0.76	98.67	96.78	100.00	100.00	95.83	91.67
1970b	−2.45	0.88	0.39	88.07	84.66	95.83	91.67	87.50	75.00
1975	−4.45	11.69	2.41	89.33	88.50	90.00	90.00	90.00	92.50
1999a	−3.11	21.90	3.92	97.48	97.10	100.00	100.00	100.00	99.18
1999b	−4.47	9.65	4.57	87.76	87.39	92.73	92.73	96.36	96.36

The first column gives the occurrence year of each event (multiple occurrences in the same year are signified as a and b, according to the occurrence date and time). The second, third and fourth columns give the minimum, maximum and mean values, respectively, of the calculated ΔCFF in bars. The fifth and sixth columns give the percentage of the rupture plane onto which ΔCFF exceeded the values of 0.0 and 0.1 bars, respectively. The last four columns give the percentage of $\Delta CFF \geq 0.1$ bar, at depths of 6, 8, 10 and 12 km, respectively

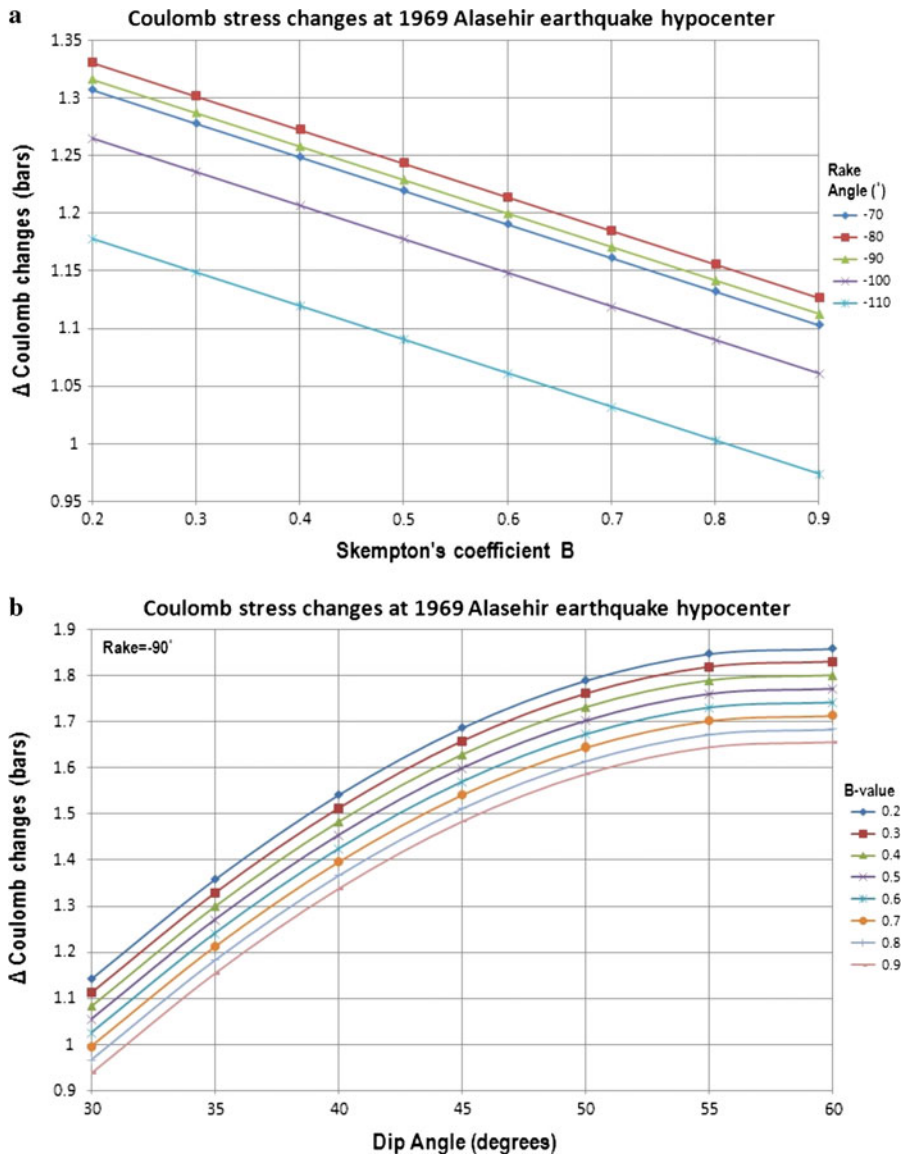

Figure 6
Changes in stress calculated at the 1969 Alaşehir hypocenter, **a** versus different values of the Skempton's coefficient (0.2–0.9) and values of rake ranging from −70° to −110°, and **b** versus different values of dip angle (30°−90°) and values of Skempton's coefficient ranging from 0.2 to 0.9

angle variance (Fig. 7a). Keeping the rake angle constant and equal to −177°, it was found that if the fault dip at Düzce hypocenter is allowed to vary from 40° to 90° the ΔCFF values may vary up to 2.1 bar (17–20% variation), whereas values up to 0.7 bar resulted from the variation of the Skempton's coefficient (7% variation) (Fig. 7b). Parsons (2005) found 20–80 and 40–50% changes for rake and dip angle variation, respectively, and 20–50% when examining the range of the values coefficient of friction.

The definition of the dip angle of the fault plane seems to play the most important role in the variations of the calculated static stress changes, since for both cases investigated these variations registered the larger values. The influence of the rake angle is still important, however, because the absolute differences found, of the order of 0.1–1.5 bars, are significant

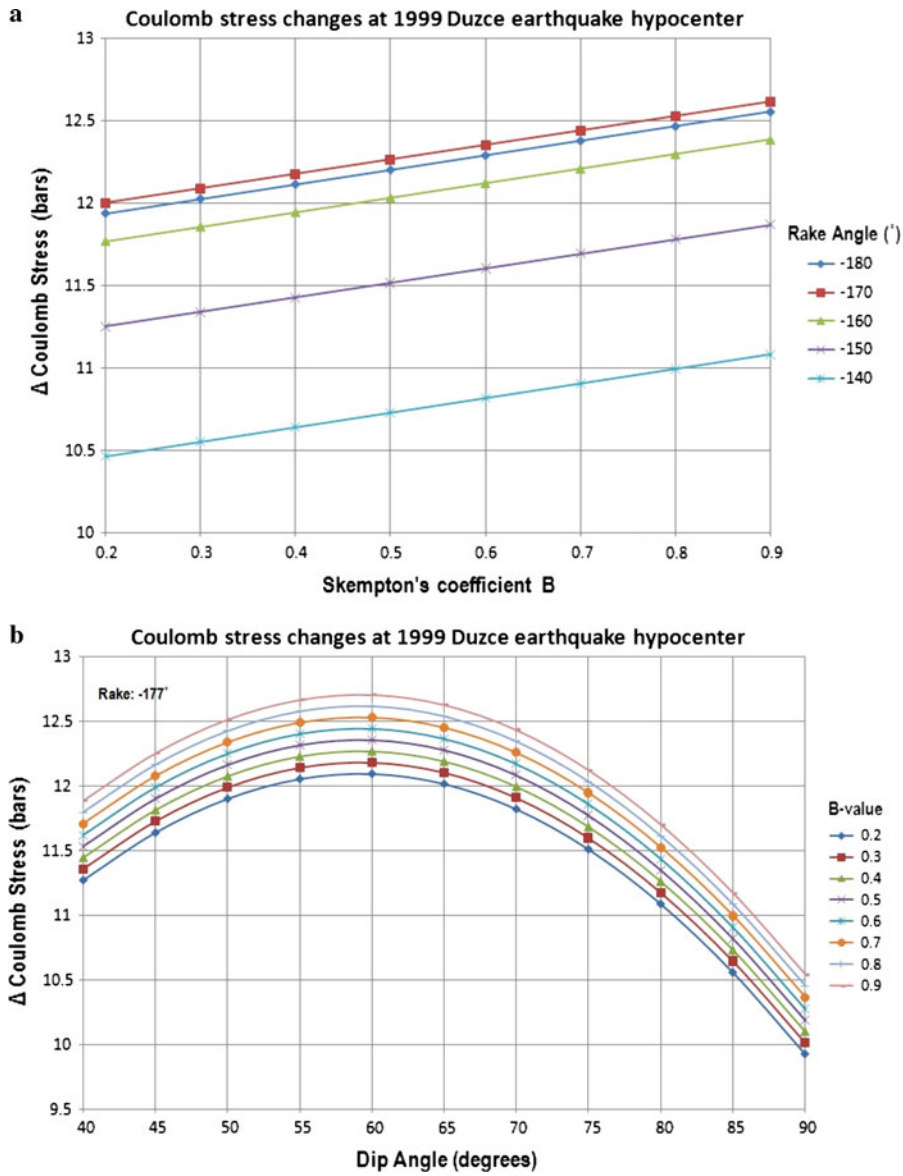

Figure 7
Changes in stress calculated at the Düzce hypocenter, **a** as a function of different values of friction coefficient from 0.1 to 0.8 and fault rakes ranging from −140° to −180°, **b** as a function of different values of Skempton's coefficient from 0.2 to 0.9 and dip angle from 40° to 90°

when triggering is inspected or when these values are incorporated in probability calculations.

7. *Stress Transfer and Earthquake Probabilities*

An attempt is made in this section to estimate probabilities for the occurrence of future strong ($M \geq 6.5$) events on the fault segments associated with events of $M \geq 6.5$ that occurred either during the instrumental period or during the past centuries and for which available information exists. For a probabilistic earthquake forecast in a region under the influence of past events it is considered that the stress transfer might hasten or delay an upcoming earthquake. Calculations of time dependent probability are a means of expressing variability in an earthquake renewal process. For this purpose we followed the

methodology of Stein *et al.* (1997), Toda *et al.* (1998) and Parsons (2004, 2005) who consider both permanent and transient effects of the stress changes on earthquake probabilities.

Two models for the estimation of earthquake probabilities are generally in use, the stationary Poisson model and the conditional probability model (Cornell *et al.*, 1968; Hagiwara, 1974). We first present results (Table 5) from the simple Poisson model for comparative purposes. This model is one that treats earthquakes as random in time (t) about an average interevent time (T_r) as:

$$P(t \le T \le t + \Delta t) = 1 - \mathrm{e}^{-\Delta t/T_r}. \qquad (8)$$

The values of T_r and the corresponding calculated probabilities are given in Table 5.

With the conditional probability model, probability can increase with time to represent increasing stress on a fault segment toward an uncertain stress threshold. A time-dependent probability (in any time interval (t, $t + \Delta t$)) is calculated by a probability density function $f(t)$ as:

$$P(t \le T \le t + \Delta t) = \int_t^{t+\Delta t} f(t)\,\mathrm{d}t, \qquad (9)$$

where P is the probability that an earthquake will occur at some time T in some interval (t, $t + \Delta t$). Two commonly applied probability density functions, $f(t)$, the lognormal distribution (e.g., Nishenko and Buland, 1987):

$$f(t, \alpha, \beta) = \frac{1}{\beta t\sqrt{2\pi}} \exp\left[\frac{-\left(\ln \frac{t}{\alpha}\right)^2}{2\beta^2}\right], \qquad (10)$$

where $\beta^2 = \ln\left(\frac{s_t^2}{T_r^2} + 1\right)$, $\alpha = \ln\left[T_r \exp(-0.5\beta^2)\right]$,, $\mathrm{T_r}$ is the average interevent time, s_t: 'the standard deviation of interevent time, and the Brownian Passage Time (Kagan and Knopoff 1987; Matthews *et al.*, 2002):

$$f(t, T_r, a) = \sqrt{\frac{T_r^2}{2\pi\alpha^2 t^3} \exp\left[\frac{-(t - T_r)^2}{2T_r\alpha^2 t}\right]}, \qquad (11)$$

where T_r is the mean interevent time and α is the aperiodicity (coefficient of variation), have characteristics that qualitatively mimic earthquake renewal. The lognormal distribution is assumed here and the mean interevent time (T_r) with the corresponding standard deviation (s_t) were estimated. For this estimation historical information is mainly taken from Papazachos and Papazachou (2003), Ambraseys and Jackson (2000) and Ambraseys (2002), whereas for some of the fault segments, and especially along the NAF, additional information on the corresponding recurrence times was taken from paleoseismological investigations. Historical information is thus enhanced, especially in cases of large events that seemed to have broken multiple segments, as the 1509 and 1766 events, or in cases of clustering, such as the three large earthquakes in 1343, 1344 and 1354, which according to Rockwell *et al.* (2001) comprise a mini-sequence rupturing much of the NAF.

In addition to the 1999 earthquake the Duzce fault (our S1 segment) is associated with the 967 and 1,878 earthquakes, with no obvious correlation with a third palaeoearthquake (1,495–1,700), result in an average recurrence time of 330–370 years (Pantosti *et al.*, 2008). The 1719 and August 1999 earthquakes both appear to have ruptured the Izmit (S3) segment with an observed interevent time of 280 years and a calculated one of 288 years (Parsons, 2004). The 1719 rupture is also supported by Pondard *et al.* (2007) and Klinger *et al.* (2003). The 1556, 1754 and 1894 earthquakes are associated with the Cinarcik (S4) segment, with an observed mean frequency of 170 years and a modeled ~250 year interevent time (Parsons, 2004). The 1754 and 1894 ruptures on Cinarcik are compatible with the most plausible scenario of rupturing by Pondard *et al.* (2007). The 1509 and the May 1766 earthquakes appear to have broken the same fault segment according to Parsons (2004), our fault segment N. Marmara (S5), giving an observed mean interevent time of 257 years and a calculated one of 270 years. The May 1766 rupture agrees with Pondard *et al.* (2007) scenario, while Klinger *et al.* (2003) assigned this event to the Izmit segment. Observations on the Ganos fault (542, 824, 1354, 1509, 1766 and 1912) support an average return period of about 275 years (Rockwell *et al.*, 2001). Parsons (2004) gives a calculated mean interevent time of 207 years. The most conservative interpretation of the trench stratigraphy and faulting evidence suggests that at least one palaeoearthquake

Table 5

Estimated 30 year probabilities on the fault segments of the study area

Segment Code Name	Tr (years)	Elapsed Time (years)	Probability before the stress step		Minimum ΔCFF (bars)	Maximum ΔCFF (bars)	Average ΔCFF (bars)	Stressing rate $\dot{\tau}$ (bars/yr)	Conditional probability after the stress step (permanent effect)			Conditional probability after the stress step (permanent + transient effect)		
			Poisson	Conditional					Minimum $P_{mod}(30)$	Maximum $P_{mod}(30)$	Average $P_{mod}(30)$	Minimum $P_{mod}(30)$	Maximum $P_{mod}(30)$	Average $P_{mod}(30)$
S1	516	9	0.0564817	8.43E−08	−24.5782	3.4056	−12.2939	0.06994	1.28E−13	2.00E−07	1.44E−10	0	0.0005081	0
S2														
S3	280	9	0.1016027	4.13E−05	−52.3904	−13.9618	−46.7524	0.17983	6.94E−10	3.40E−06	2.43E−09	0	0	0
S4	281	114	0.1012601	0.0756	0.7583	20.7883	4.562	0.2146	0.0817	0.2664	0.1148	0.0867	0.5178	0.1541
S5	141	242	0.1916547	0.3815	−0.4677	−0.3041	−0.3479	0.2583	0.3689	0.3733	0.3721	0.3691	0.3734	0.3722
S6	149	354	0.1823675	0.1096	−32.6356	5.6021	−0.6235	0.18927	0.0002266	0.1878	0.1018	0.0003309	0.1796	0.1024
S7	279	96	0.1019476	0.0536	−10.2436	−0.3658	−6.6026	0.09318	0.0013	0.0489	0.0058	7.50E−11	0.0443	7.42E−05
S8														
S9	116	33	0.2278842	0.1389	−5.4096	4.275	−3.6749	0.14403	0.0506	0.2352	0.0729	0.0005075	0.4812	0.0079
S10	274	41	0.103708	0.0043	−46.1886	−19.8572	−33.8926	0.06677	7.99E−15	5.66E−08	1.26E−11	0	0	0
S11	500	51	0.0582355	0.0001469	−84.5332	−16.0104	−29.6677	0.12638	6.66E−16	1.78E−06	2.37E−08	0	0	0
S12	495.7	153	0.0587255	0.0185	−58.6503	−1.1137	−6.3017	0.04397	0	0.0095	0.0001166	0	0.0052	9.82E−10
S13	500	153	0.0582355	0.0179	−8.0555	4.8023	0.9243	0.06091	0.000175	0.0586	0.0247	1.98E−08	0.1594	0.0326
S14	641	44	0.0457236	7.29E−06	−33.7195	−0.9043	−20.8138	0.03791	0	3.88E−06	4.11E−15	0	6.64E−08	0
S15	1013	452	0.0291808	0.0218	3.8029	73.2066	11.447	0.01973	0.1454	0.9356	0.3571	0.2529	0.9987	0.7043
S16	265	55	0.1070347	0.014	−22.4072	−0.035	−11.8283	0.02232	0	0.0135	1.69E−11	0	0.0123	0
S17	500	64	0.0582355	0.0004609	−36.6035	−12.1088	−14.9083	0.03219	0	2.60E−10	8.03E−12	0	0	0
S18	137	199	0.1966607	0.3908	−0.2629	5.6945	0.1151	0.02748	0.3242	0.977	0.4203	0.3235	0.9652	0.4205
S19	500	148	0.0582355	0.0161	−204.0237	−20.7238	−53.5348	0.03041	0	2.68E−08	0	0	0	0
S20	500	38	0.0582355	3.33E−05	−230.4551	−4.2825	−64.5768	0.0313	0	2.88E−06	0	0	0	0
S21														
S22														
S23	311.5	89	0.0918159	0.0282	−25.5562	−9.0319	−10.6422	0.03526	1.99E−08	0.0002332	9.37E−05	0	0	0
S24	500	69	0.0582355	0.000668	−52.8621	−13.1149	−19.3354	0.04078	5.00E−15	1.47E−06	6.97E−08	0	0	0
S25														
S26	560	59	0.0521618	0.0001244	−139.1693	−12.0385	−22.8667	0.03593	0	2.09E−07	5.05E−10	0	0	0
S27														
S28	500	39	0.0582355	3.79E−05	−41.0145	−7.6932	−13.0689	0.02836	0	2.28E−07	5.16E−09	0	0	0
S29	500	163	0.0582355	0.0217	−0.0461	0.6387	0.0933	0.02605	0.0211	0.0306	0.0228	0.0204	0.0447	0.0243
S30	500	128	0.0582355	0.0098	−0.8781	−0.0961	−0.4526	0.04347	0.0072	0.0095	0.0084	0.0037	0.0089	0.0061
S31	500	128	0.0582355	0.0098	−1.0768	−0.9031	−1.0313	0.04788	0.0069	0.0073	0.007	0.0033	0.004	0.0034
S32	425.5	128	0.0680772	0.0211	−1.0753	−0.4059	−0.8155	0.0399	0.0138	0.018	0.0153	0.0062	0.0139	0.0087
S33	500	125	0.0582355	0.009	−1.8369	−0.2005	−0.5217	0.04387	0.0046	0.0084	0.0075	0.0008247	0.0073	0.0051
S34	500	127	0.0582355	0.0095	−3.5359	−1.4241	−2.7912	0.04287	0.0023	0.0056	0.0032	1.80E−05	0.0016	0.0001312

Table 5 continued

Segment Code Name	Tr (years)	Elapsed Time (years)	Probability before the stress step		Minimum ΔCFF (bars)	Maximum ΔCFF (bars)	Average ΔCFF (bars)	Stressing rate $\dot{\tau}$ (bars/yr)	Conditional probability after the stress step (permanent effect)			Conditional probability after the stress step (permanent + transient effect)		
			Poisson	Conditional					Minimum $P_{mod}(30)$	Maximum $P_{mod}(30)$	Average $P_{mod}(30)$	Minimum $P_{mod}(30)$	Maximum $P_{mod}(30)$	Average $P_{mod}(30)$
S35	500	357	0.0582355	0.0923	0.0126	0.0315	0.0234	0.05287	0.0926	0.0931	0.0929	0.0926	0.0932	0.093
S36	500	306	0.0582355	0.078	−0.0538	0.0115	−0.0313	0.04618	0.0767	0.0783	0.0773	0.0764	0.0784	0.0771
S37	246	109	0.1148085	0.1041	−0.1418	4.2329	0.2102	0.04254	0.0992	0.3001	0.1116	0.0941	0.5298	0.1199
S38	500	53	0.0582355	0.0001785	−48.5545	−16.3565	−22.0164	0.04809	4.16E−13	2.72E−07	2.58E−08	0	0	0
S39														
S40	500	104	0.0582355	0.0044	−36.9901	−15.4043	−17.7095	0.03264	8.59E−13	4.77E−07	1.16E−07	0	0	0
S41														
S42														
S43	500	139	0.0582355	0.0131	−0.0831	0.4846	0.0602	0.02981	0.0126	0.0166	0.0135	0.0117	0.0237	0.0142
S44														
S45	500	52	0.0582355	0.0001621	−16.9506	−0.61	−8.4607	0.02325	1.03E−10	0.0001071	1.53E−07	0	3.46E−06	0
S46														
S47	400	75	0.0723	0.0043	−44.8297	−13.0816	−17.0323	0.03916	6.68E−13	7.36E−06	9.79E−07	0	0	0
S48														
S49														
S50														
S51	500	51	0.0582355	0.0001469	−9.339	3.5846	−4.0189	0.02571	1.39E−10	0.0007856	5.46E−07	0	0.164	0
S52	500	1590	0.0582355	0.1123	−0.4279	0.2749	−0.0141	0.02575	0.0879	0.1301	0.1114	0.0882	0.1298	0.1114
S53	500	94	0.0582355	0.0028	−28.934	10.6422	−1.8285	0.02561	5.97E−13	0.0376	0.0008495	0	0.8131	8.81E−07

The three-first columns of the table give the code name of each fault segment, the recurrence time, T_r, and the time elapsed since the occurrence of the last strong ($M \geq 6.5$) earthquake on the corresponding segment, respectively. The fourth and fifth columns give the Poissonian and Conditional probabilities. The next three columns give the minimum, maximum and average value of the accumulated Coulomb stress changes onto each fault segment, which are due to the coseismic slips of the modeled events. The ninth column gives the stressing rate of each segment in bars/year. The tenth through twelfth columns give the maximum, minimum and average probability of occurrence for the next 30 years modified by the permanent effect of ΔCFF. The last three columns give the corresponding probabilities modified by both the permanent and transient effect of ΔCFF. Calculations were not performed for the fault segments where there is no information available for the occurrence of events with $M \geq 6.5$

(most probably two) occurred after A.D. 1693 on the 1967 Mudurnu (S11) segment (Palyvos *et al.*, 2007). For the Yenice (S17) fault Kurcer *et al.* (2008) estimated a recurrence interval of 660 ± 160 years for large morphotectonic earthquakes, creating linear surface ruptures.

The paleoseismological observations were combined with information from the historical catalogs mentioned above, for events of $6.5 \leq M \leq 7.0$. In cases where only one or two events were reported for a particular fault segment, interevent times equal to 500 years and $\alpha = 0.5$ were assumed. This later value is in accordance with previous investigations in the area (Stein *et al.*, 1997; Erdik *et al.*, 2004; Parsons, 2004).

The incorporation of calculated stress changes in conditional probabilities calculations needs the treatment of a stress change as an advance or delay in the earthquake cycle. A sudden stress change should be equivalent to a sudden shift in the time, T', to the next earthquake. The 'life clock' of the fault of interest can be estimated as:

$$T' = \frac{\Delta CFF}{\dot{\tau}}, \tag{12}$$

where ΔCFF is the stress change due to the coseismic stress changes by the nearby events and $\dot{\tau}$ is the tectonic stressing rate (in bars/year). Therefore, for the calculation of the conditional probability for the fault of interest an adjusted time by the clock change is taken into account:

$$P_c(t_1) = \frac{\int_{t_1}^{t_1+\Delta t} f_t(t+T)\,\mathrm{d}t}{\int_{t_1}^{\infty} f_t(t+T)\,\mathrm{d}t}. \tag{13}$$

Stressing rates were calculated for each fault segment from the yearly slip rate and the use of the same dislocation program as for static stress change calculations. The $\dot{\tau}$ values are displayed in Table 5 and are in agreement with those from Stein *et al.* (1997) who estimated a value of 0.15 bar/year along most of the NAF system. The ΔCFF value on each fault segment was achieved by extending the calculations of the accumulated static stress changes due to the coseismic slip of the modeled events up to 2009. Since uncertainties are involved in these estimations and because stress change is spatially variable, we considered three different values, i.e. the minimum, maximum and average calculated ΔCFF values (Table 5), and consequently three different clock change values.

The next step was to estimate the rate-state transient effect that describes an expected enhanced rate of earthquake nucleation resulting from a stress increase and which can be expressed as a probability. For a stress decrease the rate of nucleation declines and eventually recovers. The time-dependent seismicity rate $R(t)$ after a stress perturbation is equal to (Dieterich, 1994):

$$R(t) = \frac{r}{[\exp(-\Delta CFF/A\sigma) - 1]\exp[-t/t_\alpha] + 1}, \tag{14}$$

where r is the steady state seismicity rate, ΔCFF is the stress step, σ is normal stress, A is a fault constitutive constant, t_α is the observed aftershock duration. The transient change in the expected earthquake rate $R(t)$ after a stress step can be related to the probability of an earthquake of a given size over the time interval Δt (we use 30 years for these computations) through a non stationary Poisson process as (Dieterich and Kilgore, 1996):

$$\begin{aligned} P(t,\Delta t) &= 1 - \exp\left[-\int_t^{\Delta t} R(t)\mathrm{d}t\right] \\ &= 1 - \exp[-N(t)], \end{aligned} \tag{15}$$

where $N(t)$ is the expected number of earthquakes in the interval Δt and is equal to:

$$N(t) = r_p\left\{\Delta t + t_\alpha \ln\left[\frac{1 + \left[\exp\left(-\frac{\Delta CFF}{A\sigma}\right) - 1\right]\exp\left[\frac{-(\Delta t)}{t_\alpha}\right]}{\exp\left(\frac{-\Delta CFF}{A\sigma}\right)}\right]\right\} \tag{16}$$

where r_p is the expected rate of earthquakes and is equal to (Toda *et al.*, 1998):

$$r_p = -\frac{1}{\Delta t}\ln[1 - P_c]. \tag{17}$$

Note that the transient effect disappears if $\Delta CFF = 0$, that is $N = r_p \cdot \Delta t$. We set the aftershock duration equal to 10% of the minimum interevent time, according to Dieterich (1994). Thus, for the area of the North Anatolian fault $t_\alpha = 25$ year,

considering a minimum return period of 250 years. For the same area a regional aftershock decay time for $M \geq 6.7$ earthquakes was found to be $\sim$35 years by PARSONS *et al*. (2000). As this duration is inversely proportional to the presumed fault stressing rate (DIETERICH, 1994) a value of $t_\alpha = 50$ year was set for the remainder of our study area. This is also in accordance with the longer observed interevent times ($\sim$500 years). Knowing the parameters t_α and ΔCFF and using the equation (DIETERICH, 1994):

$$t_\alpha = \frac{A\sigma}{\dot{\tau}} \tag{18}$$

we calculated the $A\sigma$. In summary, the net probability of events rupturing each fault segment combines both the permanent and transient effects of a stress step. Net probability is obtained by first computing the permanent effect of a stress change on the conditional probability using the approach of Eq. 13. Then the expected rate of earthquakes, r_p, for the permanent effect is obtained using Eq. 17 to evaluate Eqs. 15, 16 for the net probability. The conditional probability after the stress step (minimum, maximum and average) for the permanent effect and both the transient and permanent effects is displayed in Table 5.

The affect of the stress step in the probability estimates becomes more evident in the cases in which the fault segment has recently failed (the cases of Izmit and Duzce segments) and where a fault segment is located along strike with a previously failed segment, resulting in the positive static stress changes on the first segments. In these cases the differences between the probability estimates before and after the stress step are significant and must be included in any assessment for the future seismic hazard. As can be observed from Table 5, the fault segments adjacent to previous ruptures (segments S4, S5, S9, S15, S18, S37, S53) exhibit high estimates of time dependent probabilities, which are appreciably larger than the estimates before the stress step was considered.

8. Discussion

The present study is an effort to interpret the occurrences of strong ($M \geq 6.5$) earthquakes in the area of western Turkey and the eastern Aegean Sea and to evaluate the future seismic hazard. The methodology applied is based on a model assuming the fault interaction that led to the triggering of one event by previous ones and explains the probable mechanism of their occurrence in space and time. The stress interactions of 22 strong earthquakes ($M \geq 6.5$) that occurred since 1904 in the study area have been investigated by calculating Coulomb Stress changes (ΔCFF). We constructed a model of the evolution of stress for the time interval of 1904–2008 in order to examine if the history of cumulative changes in stress can explain the spatial and temporal occurrence of strong ($M \geq 6.5$) earthquakes in the region. Tectonic stress loading is simulated by introducing a negative virtual slip on major fault segments. From this study and from previous investigations, it has become clear that changes in Coulomb stress are associated with areas where future events are likely to occur. Thus, regions of increased stress must be considered as subject to greater hazard than anywhere else.

When considering the accumulated stress changes our calculations indicate that the Coulomb stress evolution model can successfully explain the location of strong earthquakes in the study area. Stress loading on the eastern Aegean, North Anatolian and the rest of western Turkey fault segments transform the stress acting on strike-slip and normal faults. The model satisfies our expectations in explaining the locations of the vast majority of the modeled events that are located in stress-enhanced regions, meaning that each earthquake seems to encourage the failure in the adjacent regions. For example, the calculated static stress changes following the 1912 Ganos ($M_w = 7.4$) earthquake encouraged the failure at the site of the 1975 Saros event ($M_w = 6.6$), as these two events are associated with nearby fault segments (S7 and S9, respectively) of the same dextral strike-slip faulting type. Similar evidence is presented from the 1957 Abant ($M_w = 7.0$) for the 1967 Mudurnu ($M_w = 7.2$) event (S11 and S10 segments, respectively), from the 1999 Izmit ($M_w = 7.4$) for the 1999 Düzce ($M_w = 7.2$) event (S3 and S1 segments, respectively), from the 1944 Ayvacik ($M_w = 6.8$) oblique faulting earthquake for the 1953 Yenice ($M_w = 7.2$) dextral strike-slip event (S17 and S16 segments, respectively), from the 1919 Soma ($M_w = 6.9$) for the 1939

Dikili ($M_w = 6.6$) earthquake, from the 1970 Gediz doublet (both of $M_w = 7.1$ on adjacent segments S20 and S19) and from the 1904 Samos ($M_w = 6.8$) for the 1955 Agathonisi ($M_w = 6.9$) earthquakes (S40 and S38 segments, respectively). It became evident that 12 out of 22 strong events occurred in nearby or adjacent fault segments, which means that the occurrence time of the subsequent ones most probably advanced, since the respective causative faults received positive values of static stress changes due to the coseismic slip of the preceding earthquakes.

The choice of the pore pressure model significantly influences the calculations of Coulomb stress changes caused by a shear dislocation in an elastic isotropic half-space (Beeler *et al*., 2000; Cocco and Rice, 2002). For this reason we performed our calculations by considering different values of normal stress components instead of choosing a value of apparent coefficient of friction and equality among these components. We investigated the effect of the fluid pore pressure in the modelling by considering different values for Skempton's coefficient ($B = 0.2$, $B = 0.5$ and $B = 0.9$). Differences are observed on a small scale and in particular close to the tips of the faults that failed. This investigation was accomplished for different faulting types in an attempt to examine if the current state of stress as derived from our evolutionary model, explains the location of the smaller events that occurred after 1999, when the last strong earthquake occurred. The results are encouraging because the majority of these events are located inside stress enhanced areas.

It is important to determine the hazardous segments that might generate an impeding earthquake. According to these results the fault segments of North Sea of Marmara (segments S4, S5 and S6), the smaller fault segment in Saros Gulf (S8), the Bursa segments (S12 and S13) and the Yenice1 segment (S15), on the NAF branches, have received positive static stress changes from the failure of adjacent fault segments in addition to the continuous tectonic loading. Some of the probable sites found in this study, namely the segments along the northern part of Marmara Sea and Saros Gulf, were also identified by previous investigations (Stein *et al*., 1997; Nalbant *et al*., 1998; Papadimitriou and Sykes, 2001) as contestant regions for the occurrence of a future strong earthquake. Several of the normal fault segments in the central part of the study area are currently in stress enhanced areas. It is worth noting here that although a large area is presented as continuously loading, we have to focus our attention only at the sites of the active faults.

With respect to probability estimations, the first remarkable result is that for most of the segments the renewal model based on the lognormal distribution predicts conditional probabilities of failure of these segments for the next 30 years, that are differentiated from those based on the Poisson model ranging between 3 and 23% (Table 5). These results agree with previous investigations, especially at the Marmara and Izmit region (Stein *et al*., 1997; Parsons, 2004), although the first authors found larger values with the Poisson model. For the conditional probabilities estimations we used mean interevent time equal to 500 years for some fault segments, because reliable historical information was not available. In the cases where the Poissonian probabilities are larger than the conditional ones for some fault segments, the time elapsed since the last event of $M \geq 6.5$ is shorter than the estimated mean interevent time (see Table 5). The uncertainties involved in these estimates concern the mean interevent time and the corresponding standard deviation, the aftershock duration (t_α) and the value of $A\sigma$ (we calculate the $A\sigma$ value using Eq. 18 considering that t_α is known from previous investigations).

The ΔCFF values, calculated according to the faulting type of each fault segment, where incorporated into the probability estimates, as the permanent stress effects and both the permanent and transient effects. For this purpose we considered minimum, maximum and average values of ΔCFF, as well as the minimum, maximum and average values of clock advanced or delay (Eq. 12). It is interesting to note that these values affect the estimated probabilities, by increasing them in comparison with Poissonian and conditional probability estimates when positive values of ΔCFF were found on a certain fault segment, or decreasing them in the cases of negative corresponding ΔCFF values. For example, in the Izmit fault segment, the ΔCFF effect decreases substantially the conditional probabilities (by a factor of 10^{-5}).

The stress transfer between adjacent fault segments considerably influences the probability estimates. For certain fault segments the differences between Poissonian and conditional estimates before the stress step are significantly different than those incorporated the stress step, and worthy of mention for future seismic hazard assessment. For the fault segments along the north Marmara Sea (S4 and S5) the Poissonian probabilities are found equal to 10% and 19%, respectively, while the corresponding time dependent ones are equal to 52 and 37%. The opposite but also significant consequence of the ΔCFF effect is observed for the Izmit (S3) and Duzce (S1) segments last ruptured in 1999, yielding a 30-year Poisson probability of 5% and 10%, respectively, whereas the time-dependent probabilities on these segments are $\sim 0\%$. These findings agree with Parsons (2004). The ΔCFF effect resulted in high probability estimates for normal fault segments being along strike with previous ruptures, in the central and southern part of the study area.

Acknowledgments

The paper greatly benefited from insightful comments of two anonymous reviewers and the editorial assistance of Martha Savage. The stress tensors were calculated using a program written by J. Deng (Deng and Sykes, 1997), based on the DIS3D code of S. Dunbar, which later improved (Erikson, 1986) and the expressions of G. Converse. Paradisopoulou P. M. wishes to express her sincere and profound thanks to Professor Stanislaw Lasocki and Assistant Professors Janusz Mirek and Beata Orlecka–Sikora from the Faculty of Geology, Geophysics and Environmental Protection, AGH University of Science and Technology, Krakow Poland, for many useful suggestions, ideas and assistance for the preparation of the useful application for our calculations. Part of this undertaking entailed a 2-month visit of the first author to AGH University in the frame of PENED grand. Critical reading of the manuscript by Rodolfo Console, from Istituto Nazionale Geofisica e Vulcanologia, Roma, Italy, is greatly appreciated. The GMT system (Wessel and Smith, 1998) was used to plot the figures. The first author is a grantee of the 03ED375 research project implemented within the framework of the "Reinforcement Programme of Human Research Manpower" (PENED) and co-financed by the National and Community Funds (25% from the Greek Ministry of Development-General Secretariat of Research and Technology and 75% from E.U.-European Social Fund) (Grant No. 03EΔ815 61585 23-09-05). Geophysics Department contribution 742.

Appendix: Events ($M \geq 6.5$) Included in the Stress Evolutionary Model

1904, Samos earthquake ($M_w = 6.8$): A rupture length equal to 46 km (Papazachos and Papazachou, 2003) and an average displacement of 1.2 m estimated from relation (4) were considered for this oblique normal faulting event (strike = 91°, dip = 45°, rake = −115°) for calculating the Coulomb stress changes due to its coseismic displacement.

1912, Ganos (Mürefte) earthquake ($M_w = 7.4$): This earthquake occurred between the Gulf of Saros and the Sea of Marmara at the western part of the North Anatolian Fault. The main earthquake was followed by two aftershocks, the first one ($M = 6.2$) on August 10 and the second ($M = 6.7$) on September 13 at the SE of the main shock (Papazachos and Papazachou, 2003). Maps, reports and photographs taken just after the earthquake are available (Macovei, 1912; Mihailovic, 1927, 1933). Surface expressions on the 50-km-long strike-slip fault were observed with ENE direction linking the Marmara and the Saros fault systems (Ates and Tabban, 1976; Barka 1992). The surface rupture pattern was complex with a substantial right-lateral strike-slip component (up to 3 m) (Ambraseys and Finkel, 1987). Nalbant *et al*. (1998) modeled this event with a rupture length of 90 km extended the rupture seen on land by 15 km to the east and 25 km to the west. Papadimitriou and Sykes (2001) use 110 km length and 3.32 m slip derived from scaling laws. In the present study a rupture equal to 116 km and an average slip of 2.8 m were estimated from Eqs. 5 to 6, respectively.

1914, Burdur earthquake ($M_w = 7.0$): This event occurred near the Burdur Lake and is associated with

a 52-km-long normal fault (strike = 230°, dip = 35°, rake = −105°) dipping to NW (PAPAZACHOS and PAPAZACHOU, 2003), with a calculated mean displacement of 1.66 m (Eq. 4).

1919, Soma earthquake ($M_w = 6.9$): This earthquake occurred at Bakircay Graben (strike = 25$\mathring{3}$, dip = 4$\mathring{5}$, rake = −11$\mathring{5}$, TAYMAZ *et al*., 1991b) on a segment adjacent to the 1939 rupture. A 43-km-fault length was estimated from relation (3) and a mean displacement of 0.63 m from the event's scalar moment.

1928, Torbali earthquake ($M_w = 6.5$): This earthquake caused considerable damage in Torbali, Izmir and Kücük Menderes Graben (PAPAZACHOS and PAPAZACHOU, 2003). It is associated with a normal fault (strike = 83°, dip = 45°, rake = −94°) with 25-km length and a mean displacement of 0.72 m calculated by using Eqs. 3 and 4.

1933, Kos earthquake ($M_w = 6.6$): This earthquake is associated with a fault segment almost parallel to the south coastline of the Kos Island (strike = 65°, dip = 50°, rake = −90°). An average displacement of 0.85 m and a fault length equal to 28 km were estimated using Eqs. 4 and 5, respectively.

1939, Dikili earthquake ($M_w = 6.6$): The Dikili earthquake occurred near the coastal Aegean area south of the Edremit Gulf. The isoseismal maps indicate that this event was located at the western extremity of the Bakırcay Graben, a normal fault zone (ARPAT and BINGÖL, 1969; WESTAWAY, 1990). The event is associated with a NE–SW trending normal faulting dipping to the north (strike = 211°, dip = 45°, rake = −115°). An estimated coseismic displacement of 0.85 m and a rupture length of 26 km were assigned for this event, from Eqs. 4 and 3, respectively.

1944, Ayvacık earthquake ($M_w = 6.8$): The earthquake occurred near the Edremit Gulf, where the southern branch of the North Anatolian Fault reaches the Aegean Sea through the Edremit Gulf (strike = 74°, dip = 46°, rake = −114° after TAYMAZ *et al*., 1991b). A fault length equal to 35 km and an average displacement equal to 1.4 m were estimated from Eqs. 3 and 4, respectively.

1949, Chios earthquake ($M_w = 6.7$): This earthquake occurred to the north of Chios Island, associated with normal faulting (strike = 84°, dip = 36°, rake = −80°) with an estimated fault length of 31 km, from scaling law (3), and a mean coseismic displacement equal to 1.03 m (Eq. 4).

1953, Yenice earthquake ($M_w = 7.2$): The Yenice earthquake occurred between the Sea of Marmara to the north and the Edremit Gulf to the south. The rupture took place at the southern branch of NAF over 60 km (PINAR, 1952; AMBRASEYS, 1970). The earthquake focal mechanism parameters (MCKENZIE, 1972; TAYMAZ *et al*., 1991a) indicate pure southwest–northeast trending right-lateral strike-slip faulting (strike = 250°, dip = 70°, rake = −160°). The slip reaches 3.5 m in the eastern part and diminishes to 1.5 m at both ends (KETIN and ROESLI, 1953; AMBRASEYS, 1970). NALBANT *et al*. (1998) modeled this event using the observed slip distribution and the geometry (length of 60 km) of the mapped surface rupture. Based on the above information the fault length is taken equal to 60 km and the mean displacement, derived from the event's scalar moment, is equal to 3.78 m.

1955, Agathonisi earthquake ($M_w = 6.9$): The earthquake occurred in the Büyük Menderes graben, near Agathonisi Island. The focal mechanism (MCKENZIE, 1972) shows NE–SW normal faulting (strike = 55°, dip = 51°, rake = −113°). We have modeled this event using a 38-km-fault length with a mean displacement of 1.19 m (Eqs. 3, 4, respectively).

1956, Amorgos earthquake ($M_w = 7.7$): This is the strongest event that occurred in the backarc Aegean area during the instrumental era. It occurred on an ENE-trending normal fault that is seated parallel to the Island's southern coastline and was followed by a strong event in an adjacent fault to its southwest, which most probably was triggered by the first occurrence. Its fault plane solution (strike = 65°, dip = 40°, rake = −90°) was determined by SHIROKOVA (1972). A fault length of 75 km, in accordance with the submarine topography, and a mean displacement of 5.30 m, were estimated for this large earthquake from Eqs. 3 and 4, respectively.

1957, Rhodes earthquake ($M_w = 7.2$): A preshock ($M = 6.8$) took place before the main earthquake ($M = 7.2$) near the Rhodes Island and many aftershocks followed, from which the largest one registered magnitude $M = 6.1$ (PAPAZACHOS and

Papazachou, 2003). The main shock is associated with a left-lateral strike-slip faulting with a NE–SW strike direction (strike = 30°, dip = 80°, rake = −41°). The fault length is estimated equal to 67 km from Eq. 5 and the mean displacement equal to 1.34 m from Eq. 6.

1957, Abant earthquake ($M_w = 7.0$): The Abant event occurred on the North Anatolian fault at the eastern part of the study area. The 40-km-long surface faulting was mapped by Ambraseys (1970). The focal mechanism (McKenzie, 1972; Taymaz *et al*., 1991a) indicates strike-slip faulting (strike = 265°, dip = 78°, rake = 179°). The slip is not well constrained, being measured at only two localities (1.4 and 1.6 m). Taking into account the morphology, a fault length of 40 km was estimated from Eq. 5 in accordance with the morphology, and a mean displacement of 1.47 was calculated from (6), in good agreement with the reported values.

1964, Manyas earthquake ($M_w = 6.9$): The Manyas earthquake occurred at the south of the Sea of Marmara in the southern branch of NAF between the Lakes Manyas and Uluabat. The focal mechanism (strike = 280°, dip = 45°, rake = −90°) (Taymaz *et al*., 1991b) indicates a WNW–ESE normal faulting although strike-slip faulting prevails in this part of our study area. The 40-km surface normal faulting (Nalbant *et al*., 1998) (*en echelon* surface rupture and fissuring over a wide zone) was interpreted as resulting from the right-lateral strike-slip motion (Erentöz and Kurtman, 1965; Ketin, 1966). A 35-km-long WNW–ESE normal fault dipping to the north is considered here with a mean displacement of 1.4 m (Eq. 6).

1967, Mudurnu earthquake ($M_w = 7.2$): The Mudurnu earthquake occurred on the NAF at the easternmost part of the Sea of Marmara, Mudurnu Valley, and extended towards the west. Its fault plane solution (strike = 275°, dip = 45°, rake = −178°) based on teleseismic body-waveform (P- and SH-) inversion (Taymaz *et al*., 1991a) shows a E–W dextral strike-slip faulting mechanism. A large aftershock (July 30, 1967, $m_b = 5.6$) occurred at its western extremity with NW–SE striking and normal fault plane solution (Stewart and Kanamori, 1982; McKenzie, 1972; Jackson and McKenzie, 1984). This illustrates the change on the NAF in this area between strike–slip motion to the east and normal and strike–slip motion on several branches to the west. Nalbant *et al*. (1998) used detailed maps of the 80-km-long surface rupture and the fault slip distribution for the event modeling (Ambraseys and Zatopek, 1969; Güçlü, 1969) which is greatest, 2.5 m, in the east and decreases steadily to the west. A fault length of 80 km is taken and a calculated mean displacement from Eq. 6, equal to 2.02 m.

1969, Alaşehir earthquake ($M_w = 6.6$): The Alaşehir earthquake occurred in the Gediz River Valley, associated with about 30–36 km of surface rupture and extending from NW through Alaşehir to SE (Ambraseys and Tchalenko, 1972). The strike of the surface varied from N85°W in the NW to N50°W in the SE (Ketin and Abdussselamoğlu 1969). Displacements at the surface measured an average of about 20 cm. The fault plane solution of the main earthquake shows a normal faulting with a dip of 32°NNE and a strike of N79°W, consistent with the strike observed at the NW end of surface ruptures (Eyidoğan and Jackson, 1985; Braunmiller and Nabelek, 1996). We model this event using the reported fault plane solution of Eyidoğan and Jackson (1985) (strike = 281°, dip = 34°, rake = −90°) as a normal fault with a length of 25 km, estimated from the Eqs. 3, and a mean displacement of 0.61 m, from Eq. 4.

1970, Gediz earthquakes ($M_w = 7.1$): About 45 km of complicated surface normal faulting was associated with this earthquake, trending both NNW–SSE and E–W down thrown to the east and north (Ambraseys and Tchalenko, 1972). The aftershock sequence defined a 40-km-wide, 200-km-long, E–W zone (Ambraseys and Tchalenko, 1972). The observed seismograms show complexity and were modeled using three main subevents (Eyidoğan and Jackson, 1985). The first subevent occurred on a 15-km-long NNW–SSE segment with a mean displacement of 1.6 m and a dip of 35°. The second subevent, of the same magnitude (M_w 7.1), triggered by the first shock and ruptured about the 24-km-long E–W segment with a mean displacement of 2.4 m and a dip pf 35°. The third subevent, much smaller in magnitude (M 5.7), occurred on a ∼15° dipping fault extending the second fault segment from 12.5 to 17.5 km depth (Eyidoğan and Jackson, 1985). We modeled this event as comprising the two major subevents.

1975, Saros earthquake ($M_w = 6.6$): The Saros segment is located in the prolongation of the Ganos (Gaziköy) fault zone at the western part of the North Anatolian Fault, where the 1975 earthquake occurred. It is an oblique right-lateral strike-slip fault as the focal mechanism indicates (strike = 68°, dip = 55°, rake = −145°) (TAYMAZ *et al*., 1991a) with ENE–WSW strike consistent with the orientation of NAF at this particular location. The rupture length is taken equal to 40 km and the mean displacement equal to 0.86 m from Eqs. 5 and 6, respectively.

1999 Izmit (Kocaeli) earthquake ($M_w = 7.4$): The Izmit earthquake, one of the most destructive earthquakes in Turkey, occurred at the western part of NAF. About 115 km of surface strike-slip faulting was associated with its occurrence, trending E–W from Sapanca–Akyazi at the east to Hersek Delta to the west (BARKA *et al*., 2002). A rupture constituted from four segments (with lengths equal to 35, 20, 26 and 35 km, going from west to east) is considered for modeling this event, according to BARKA *et al*. (2002). Details of the geometry and coseismic slip of each segment are given in Table 2.

1999 Düzce earthquake ($M_w = 7.2$): This event occurred in Bolü basin, in the adjacent fault segment associated with the previous Izmit earthquake and with in <3 months afterwards. The fault length is about 40–56 km long (KIRATZI and LOUVARI, 2001; AKYÜZ *et al*., 2002; AYDIN and KALAFAT, 2002) and the focal mechanism indicates a right-lateral strike-slip faulting with E–W strike and dip to the north (strike = 262°, dip = 53°, rake = −177°). We model this event according to KIRATZI and LOUVARI (2001), who suggested a fault length of 56 km and a mean displacement of 2.60 m.

REFERENCES

AKYÜZ, H. S., HARTLEB, R., BARKA, A., ALTUNEL, E., SUNAL, G., MEYER, B., and ARMIJO, R. (2002), *Surface rupture and slip distribution of the November 1999 Düzce earthquake (M = 7.1), North Anatolian Fault, Bolu, Turkey*, Bull. Seismol. Soc. Am. *92*, 61–66.

AMBRASEYS, N. N. (1970), *Some characteristic features of the North Anatolian fault zone*, Tectonophysics *9*, 143–165.

AMBRASEYS, N. N. (2001), *Reassesment of earthquakes, 1900–1999, in the Eastern Mediterranean and the Middle East*, Geophys. J. Int. *145*, 471–485.

AMBRASEYS, N. N. (2002), *The seismic activity of the Marmara Sea region over the last 2000 years*, Bull. Seismol. Soc. Am. *92*, 1–18.

AMBRASEYS, N. N. and ZATOPEK, A. (1969), *The Mudurnu Valley, west Anatolia, Turkey, earthquake of 22 July, 1967*, Bull. Seismol. Soc. Am. *59*, 521–589.

AMBRASEYS, N. N. and TCHALENKO, J. S. (1972), *Seismotectonic aspects of the Gediz, Turkey, earthquake of March 1970*, Geophys. J. R. Astron. Soc. *30*, 229–252.

AMBRASEYS, N. N. and FINKEL, C. (1987), *The Saros–Marmara earthquake of 9 August, 1912*, Earthq. Eng. Struct. Dyn. *15*, 189–211.

AMBRASEYS, N. N. and JACKSON, J. A. (1990), *Seismicity and associated strain of central Greece between 1890 and 1988*, Geophys. J. Int. *101*, 663–708.

AMBRASEYS, N. N. and JACKSON, J. A. (2000), *Seismicity of Marmara (Turkey) since 1500*, Geophys. J. Int. *141*, F1–F6.

ARMIJO, R., MEYER, B., HUBERT, A., and BARKA, A. (1999), *Propagation of the North Anatolian fault into the north Aegean: Timing and kinematics*, Geology *27*, 267–270.

ARMIJO, R., FLERIT, F., KING, G. and MEYER, B. (2003), *Linear elastic fracture mechanics explains the past and present evolution of the Aegean*, Earth Plan. Sci. Lett. *217*, 85–95.

ARPAT, E. and BINGÖL, E. (1969), *The rift system of western Turkey, through on its development*, Bull. Miner. Res. Expl. I. *73*, 1–9.

ATES, R. and TABBAN, A. (1976), *A preliminary report on August 9, 1912 Mürefte–Sarköy earthquake (in Turkish)*, Earthquake Res. Inst. Ankara, Turkey.

AYDIN, A. and KALAFAT, D. (2002), *Surface ruptures of the August 17 and November 12, 1999, Izmit, and Duzce Earthquakes in NW Anatolia*, Turkey: Their tectonic and kinematic significance and the associated damage, Bull. Seismol. Soc. Am. *92*, 95–106.

AYHAN, M. E., BURGMANN, R., MCCLUSKY S., LENK, O., AKTUG, B., HERECE, E., and REILINGER, R. E. (2001), *Kinematics of the $M_w = 7.2$, 12 November, 1999*, Duzce, Turkey Earthquake, Geophys. Res. Lett. *28*, 367–370.

BARKA, A. A. (1992), *The North Anatolian fault*, Ann. Tectonicae *6*, 164–195.

BARKA, A. A., AKYÜZ, H. S., ALTUNEL, E., SUNAL, G., ÇAKIR, Z., DIKBAS, A., YELI, B., ARMIJO, R., MEYER, B., J. B. DE CHABALIER, ROKWELL, T., DOLAN, J. R., HARTLEB, R., DAWSON, T., CHRISTOFFERSON, S., TUCKER, A., FUMAL, T., LANGRIDGE, R., STENNER, H., LETTIS, W., BACHHUBER, J., and PAGE, W. (2002), *The surface rupture and slip distribution of the 17 August, 1999 İzmit earthquake, M = 7.4, North Anatolian Fault*, Bull. Seismol. Soc. Am. *92*, 43–60.

BEELER, N. M., SIMPSON, R. W., HICKMAN, S. H., and LOCKNER, D. A. (2000), *Pore fluid pressure, apparent friction, and Coulomb failure*, J. Geophys. Res. *105*, 25533–25542.

BIRD, P. and KAGAN, Y. Y. (2004), *Plate–tectonic analysis of shallow seismicity: Apparent boundary width, beta, corner magnitude, coupled lithosphere thickness, and coupling in seven tectonic settings*, Bull. Seismol. Soc. Am. *94*, 2380–2399.

Bozkurt, E. (2001), Neotectonics of Turkey–a synthesis, Geodynamica Acta *14*, 3–30.

BOZKURT, E. (2003), *Origin of the NE–trending basins in western Turkey*, Geodynamica Acta *16*, 61–81.

BRAUNMILLER, J. and NABELEK, J. (1996), *Geometry of continental normal faults: Seismological constraints*, J. Geophys. Res. *101*, 3045–3052.

Cocco, M. and Rice, J. R. (2002), *Pore pressure and poroelasticity effects in Coulomb stress analysis of earthquake interactions*, J. Geophys. Res. *107*, doi:10.1029/2000JB000138.

Cornell, C. A., Wu, S.-C., Winterstein, S. R., Dietrich, J. H., and Simpson, R. W. (1968), *Seismic hazard induced by mechanically interactive fault segments*, Bull. Seismol. Soc. Am. *83*, 436–449.

Davies, R., England, P., Parsons, B., Billiris, H., Paradissis, D., and Veis, G. (1997), *Geodetic strain of Greece in the interval 1892–1992*, J. Geophys. Res. *102*, 24,571–24,588.

Deng, J. and Sykes, L. (1997), *Evolution of the stress field in Southern California and triggering of moderate size earthquakes: A 200–year perspective,* J. Geophys. Res. *102*, 9859–9886.

Dieterich, J. H. (1994), *A constitutive law for rate of earthquake production and its application to earthquake clustering*, J. Geophys. Res. *99*, 2601–2618.

Dieterich, J. H. and Kilgore, B. (1996), *Implications of fault constitutive properties for earthquake prediction*, Proc. Natl. Acad. Sci. USA *93*, 3787–3794.

Erdik, M., Demircioglu, M., Sesetyan, K., Durukal, E., and Siyahi, B. (2004), *Earthquake hazard in Marmara region, Turkey*, Soil Dyn. Earth. Eng. *24*, 605–631.

Erentöz, C. and Kurtman, F. (1965), *A report on the 1964 Manyas earthquake (in Turkish)*, Bull. Miner. Res. Expl. Inst. *63*, 1–5.

Erikson, L. (1986), *User's Manual for DIS3D: A three-dimensional dislocation program with applications to faulting in the Earth*, Masters Thesis, Stanford Univ., Stanford, California, pp. 167.

Eyidoğan, H. (1988), *Rates of crustal deformation in western Turkey as deduced from major earthquakes*, Tectonophysics *148*, 83–92.

Eyidoğan, H. and Jackson, J. (1985*), A seismological study of normal faulting in the Demirci, Alasehir and Gediz earthquakes of 1969–70 in western Turkey: Implications for the nature and geometry of deformation in the continental crust*, Geophys. J. R. Astron. Soc. *81*, 569–607.

Flerit, F., Armijo, R., King. G., and Meyer, B. (2004), *The mechanical interaction between the propagating North Anatolian fault and the backarc extension in the Aegean*, Earth Planet. Sci. Lett. *224*, 347–362.

Güçlü, U., *Section 1: Field investigation (in Turkish), in Investigations on July 22, 1967 Mudurnu Valley earthquake* (ed. Ergin K.) (Publ. 27, Istanbul Technical University, Earth Physics Institute, Istanbul, Turkey, 1969) pp. 1–27.

Hagiwara, Y. (1974), *Probability of earthquake occurrence as obtained from a Weibull distribution analysis of crustal strain*, Tectonophysics *23*, 313–318.

Hardebeck, J. L. (2004), *Stress triggering and earthquake probability estimates*, J. Geophys. Res. *109*, B04310, doi:10.1029/2003JB002437.

Harris, R. (1998), *Introduction to special section: Stress triggers, stress shadows, and implications for seismic hazard*, J. Geophys. Res. *103*, 251–254.

Harris, R. and Simpson, R. (1993), *In the shadow of 1857: An evaluation of the static stress changes generated by the M 8 Ft. Tejon, California, earthquake*, EOS, Trans. Am. Geophys. Un. *74*(43), 427.

Harris, R. and Simpson, R. (1996), *In the shadow of 1857: The effect of the great Ft Tejon earthquake on subsequent earthquakes in Southern California*, Geophys. Res. Lett. *23*, 229–232.

Hubert-Ferrari, A., Barka, A., Jaques, E., Nalbant, S. S., Meyer, B., Armijo, R., Tapponnier, P., and King G. C. P. (2000), *Seismic hazard in the Marmara Sea region following the 17 August, 1999 Izmit earthquake*, Nature *404*, 269–273.

Jackson, J. (1994), *Active tectonics of the Aegean region*, Ann. Rev. Earth Planet. Sci. *22*, 239–271.

Jackson, J. and McKenzie, D. P. (1984), *Active tectonics of the Alpine–Himalayan Belt between western Turkey and Pakistan*, Geophys. J. R. Astron. Soc. *77*, 185–246.

Jackson, J., Hains, A. J., and Holt, W. E. (1994), *A comparison of satellite laser ranging and seismicity data in the Aegean region*, Geophys. Res. Lett. *21*, 2849–2852.

Kagan, Y. Y. and L. Knopoff (1987), *Random stress and earthquake statistics: Time dependence*, Geophys. J. R. Astron. Soc. *88*, 723–731.

Ketin, İ. (1966), *Tension cracks occurred on the surface during the October 6, 1964 Manyas earthquake (in Turkish)*, Bull. Turk. Geol. Union *10*, 44–51.

Ketin, İ. and Roesli, T. (1953), *Macroseismic research of the Northwest Anatolian earthquake of the 18 March 1953 (in German)*, Eclogae Geol. Helv. *46*, 187–208.

Ketin, İ. and Abdussselamoğlu, S. (1969), *Macroseismic observations on March 23, 1969 Demirci and March 28, 1969 Alasehir–Sarigöl earthquakes (in Turkish)*, Min. Mag. Istanbul Univ. *4*(5), 21–26.

King, G. C. P., Oppenheimer, D., and Amelung, F. (1994), *Block versus continuum deformation in the western United States*, Earth Planet. Sc. Lett. *128*, 55–64.

King, G. C. P., Hubert–Ferrari, A., Nalbant, S. S., Meyer, B., Armijo, R., and Bowman, D. (2001), *Coulomb interactions and the 17 August, 1999 Izmit, Turkey earthquake*, Earth and Planet. Sci., C. R. Acad. Sci. Paris *333*, 557–569.

Kiratzi, A.A. and Louvari, E. (2001), *Source parameters of the Izmit–Bolu 1999 (Turkey) earthquake sequences from teleseismic data*, Annali di Geofisica *44*, 33–47.

Klinger, Y., Sieh, K., Altunel, E., Akoglu, A., Barka, A., Dawson, T., Gonzalez, T., Meltzner, A., and Rockwell, T. (2003), *Paleoseismic evidence of characteristic slip on the western segment of the North Anatolian Fault*, Turkey, Bull. Seismol. Soc. Am. *93*, 2317–2332.

Kurcer, A., Chatzipetros, A., Tutkun, S. Z., Pavlides, S., Ates, O., and Valkaniotis, S. (2008), *The Yenice–Gonen active fault (NW Turkey): Active tectonics and palaeoseismology*, Tectonophysics *453*, 263–275.

Macovei, G. (1912), *About the Sea of Marmara earthquake of the 9 August, 1912 (in French)*, Bull. Sect. Acad. Roumanie, Bucarest *1* (1), pp. 1–10.

Matthews, M. V., Ellsworth, W. L., and Reasenberg, P. A. (2002), *A Brownian model for recurrent earthquakes*, Bull. Seismol. Soc. Am. *92*, 2233–2250.

McClusky, S., Balassanian, S., Barka, A., Demir, C., Ergintav, S., Georgiev, I., Gurkan, O., Hamburger, M., Hurst, K., Kahle, H., Kastens, K., Kekelidze, G., King, R., Kotzev, V., Lenk, O., Mahmoud, S., Mishin, A., Nadariya, M., Ouzounis, A., Paradissis, D., Peter, Y., Prilepin, M., Reilinger, R., Sanli, I., Seeger, H., Tealeb, A., Toksoz, M.N., and Veis, G. (2000), *Global positioning system constraints on plate kinematics and dynamics in the eastern Mediterranean and Caucasus*, J. Geophys. Res. *105*, 5695–5719.

McClusky, S., Reilinger, R., Mahmoud, S., Ben–sari, D., and Tealeb, A. (2003), *GPS constraints on Africa (Nubia) and Arabia plate motions*, Geophys. J. Intern. *155*, 126–138.

McKenzie, D. P. (1970), *The plate tectonics of the Mediterranean region*, Nature *226*, 271–299.

McKenzie, D. P. (1972), *Active tectonics of the Mediterranean region*, Geophys. J. R. Astron. Soc. *30*, 109–185.

Mihailovic, J. (1927), *The large seismic disasters around the Sea of Marmara (in French)*, Inst. Seismol. De l' Univ. de Belgrade, Belgrade, Yugoslavia.

Mihailovic, J. (1933), *The seismicity of the Sea of Marmara and Asia minor (in French)*, Monogr. Trav. Sci. Inst. Seismol., 2B.

Nalbant, S. S., Hubert, A., and King, G. C. P. (1998), *Stress coupling between earthquakes in northwest Turkey and the north Aegean Sea*, J. Geophys. Res. *103*, 469–486.

Nishenko, S. P. and Buland R. (1987), *A generic recurrence interval distribution for earthquake forecasting*, Bull. Seismol. Soc. Am. *77*, 1382–1399.

Nyst, M. and Thatcher, W., (2004), *New constraints on the active tectonic deformation of the Aegean*, J. Geophys. Res. *109*, B11406, doi:10.1029/2003JB002830.

Okada, Y. (1992), *Internal deformation due to shear and tensile faults in a half–space*, Bull. Seismol. Soc. Am. *82*, 1018–1040.

Pacheco, J. F. and Sykes, L. R. (1992), *Seismic moment catalogue of large shallow earthquakes, 1900 to 1989*, Bull. Seismol. Soc. Am. *82*, 1306–1349.

Palyvos, N., Pantosti, D., Zabci, C., and D' Addezio, G. (2007), *Paleoseismological evidence of recent earthquakes on the 1967 Mudurnu valley earthquake segment of the North Anatolian Fault zone*, Bull. Seismol. Soc. Am. *97*, 1646–1661.

Pantosti, D., Pucci, S., Palyvos, N., De Martini, P. M., D' Addezio, G., Collins, P. E. F., and Zabci, C. (2008), *Paleoearthquakes of the Düzce fault (North Anatolian Fault Zone): Insights for large surface faulting earthquake recurrence*, J. Geophys. Res. *113*, doi:10.1029/2006JB004679.

Papadimitriou, E. E. and Sykes, L. R. (2001), *Evolution of the stress field in the northern Aegean Sea (Greece)*, Geophys. J. Int. *146*, 747–759.

Papadimitriou, E.E., Karakostas, V., and Papazachos, B. C. (2001), *Rupture zones in the area of the 17.08.99 Izmit (NW Turkey) large earthquake (M_w 7.4) and stress changes caused by its generation*, J. Seismol. *5*, 269–276.

Papadimitriou, E. E., Sourlas, G., and Karakostas, V. G. (2005), Seismicity variations in southern Aegean, Greece, before and after the large (M_w 7.7) 1956 Amorgos earthquake due to evolving stress, Pure Appl. Geophys. *162*, 783–804.

Papazachos, B. C. and Comninakis, P. E. (1969), *Geophysical features of the Greek Island Arc and Eastern Mediterranean Ridge,* Com. Ren. Séances Conf. Reunie Madrid, *16*, 74–75.

Papazachos, B. C. and Comninakis, P. E. (1971), *Geophysical and tectonic features of the Aegean arc*, J. Geophys. Res. *76*, 8517–8533.

Papazachos, B. C. and Papazachou, C. (2003), *The earthquakes of Greece, Ziti publications, Thessaloniki*, pp. 289.

Papazachos, B. C., Kiratzi, A. A., Hatzidimitriou, P. M., and Rocca, A. Ch. (1984), *Seismic faults in the Aegean area,* Tectonophysics *106*, 71–85.

Papazachos, B. C., Kiratzi, A. A., and Karakostas, B. G. (1997), *Toward a homogeneous moment magnitude determination in Greece and surrounding area*, Bull. Seismol. Soc. Am. *87*, 474–483.

Papazachos, B. C., Papadimitriou, E. E., Kiratzi A. A., Papazachos, C. B., and Louvari, E. K. (1998), *Fault plane solutions in the Aegean Sea and the surrounding area and their tectonic implications*, Bull. Geof. Teor. Appl. *39*, 199–218.

Papazachos, B. C., Scordilis, E. M., Panagiotopoulos, D. G., Papazachos, C. B., and Karakaisis, G. F. (2004), *Global Relations between seismic fault parameters and moment magnitude of Earthquakes*, Bull. Geol. Soc. Greece XXXVI, 1482–1489.

Papazachos, C. (1999), *Seismological and GPS evidence for the Aegean Anatolia interaction*, Geophys. Res. Lett. *17*, 2653–2656.

Parsons, T. (2004), *Recalculated probability of $M \geq 7$ earthquakes beneath the Sea of Marmara*, Turkey, J. Geophys. Res. *109*, doi:10.1029/2003JB002667.

Parsons, T. (2005), *Significance of stress transfer in time–dependent earthquake probability calculations*, J. Geophys Res. *110*, doi:10.1029/2004JB003190.

Parsons, T., Toda, S., Stein, R. S., Barka, A., and Dieterich, J. H. (2000), *Heightened odds of large earthquakes near Istanbul: An interaction–based probability calculation*, Science *288*, 661–665.

Pinar, N. (1952), *The Yenice earthquake of the 18 March, 1953 and the fracture line of Yenice–Gönen*, Rev. Fac. Sci. Univ. Istanbul, Ser. A., *18*, 131–141.

Pondard, N., Armijo, R., King, G. C. P., Meyer, B., and Flerit, F. (2007), *Fault interactions in the Sea of Marmara pull–apart (North Anatolian Fault): Earthquake clustering and propagating earthquake sequences*, Geophys. J. Int. *171*, 1185–1197.

Reilinger, R. E., McClusky, S. C., Oral M. B., King, R. W., King, R. W., and Toksöz, M. N. (1997), *Global Positioning System measurements of present–day crustal movements in the Arabia–Africa–Eurasia plate collision zone*, J. Geophys Res. *102*, 983–999.

Reilinger, R., McClusky, S., Vernant, P., Lawrence, S., Ergintav, S., Cakmak, R., Ozener, H., Kadirov, F., Guliev, I., Stepanyan, R., Nadariya, M., Hahubia, G., Mahmoud, S., Sakr, K., ArRajehi, A., Paradissis, D., Al–Aydrus, A., Prilepin, M., Guseva, T., Evren, E., Dmitrotsa, A., Filikov, S. V., Gomez, F., Al–Ghazzi R., and Karam, G. (2006), *GPS constraints on continental deformation in the Africa–Arabia–Eurasia continental collision zone and implications for the dynamics of plate interactions*, J. Geophys. Res. *111*, doi:10.1029/2005JB004051.

Rice, J. R. and Clearly, M. P. (1976), *Some basic stress diffusion solutions fro fluid–saturated elastic porous media with compressible constituents*, Rev. Geophys. *14*, 227–241.

Robinson, R. and McGinty, P. J. (2000), *The enigma of the Arthur's Pass, New Zealand, earthquake. 2. The aftershock distribution and its relation to regional and induced stress fields*, J. Geophys. Res. *105*, 16139–16150.

Rockwell, T., Barka, A., Dawson, T., Akyuz, S., and Thorup, K. (2001), *Paleoseismology of the Gazikoy–Saros segment of the North Anatolia fault, northwestern Turkey: Comparison of the historical and paleoseismic records, implications of regional seismic hazard, and models of earthquake recurrence*, J. Seismology *5*, 433–448.

Saunders, P., Priestley, K., and Taymaz, T. (1998), *Variations in the crustal structure beneath western Turkey*, Geophys. J. Intern. *134*, 373–389.

Seyitoğlu, G. and Scott, B. C. (1991), *Late Cenozoic crustal extension and basin formation in west Turkey*, Geol. Mag. *128*, 155–166.

Shirokova, E. (1972), *Stress pattern and probable motion in the earthquake foci of the Asia-Mediterranean seismic belt, in elastic strain field of the Earth and mechanisms of earthquake sources.* In L. M. Balakina et al. (eds.), Nauka, Moscow, 8.

STEIN, R. S. (1999), *The role of stress transfer in earthquake occurrence*, Nature *402*, 605–609.

STEIN, R. S., BARKA, A. A., and DIETERICH, J. H. (1997), *Progressive failure on the North Anatolian fault since 1939 by earthquakes stress triggering*, Geophys. J. Int. *128*, 594–604.

STEWART, S. G. and KANAMORI, H. (1982), *Complexity of rupture in large strike–slip earthquakes in Turkey*, Phys. Earth Planet. Inter. *28*, 70–84.

TAYMAZ, T. (1990), *Earthquake source parameters in the Eastern Mediterranean Region, Ph.D. Thesis, Darwin College*, University of Cambridge, UK, 244 pp.

TAYMAZ, T. (1996), *S–P–wave travel-time residuals from earthquakes and lateral heterogeneity in the upper mantle beneath the Aegean and the Hellenic Trench near Crete*, Geophys. J. Int. *127*, 545–558.

TAYMAZ, T., and PRICE, S. (1992), *The 1971 May 12 Burdur earthquake sequence, SW Turkey: A synthesis of seismological and geological observations*, Geophys. J. Int. *108*, 589–603.

TAYMAZ, T., JACKSON, J. A., and MCKENZIE, D. P. (1991a), *Active tectonics of the North and Central Aegean Sea*, Geophys. J. Int. *106*, 433–490.

TAYMAZ, T., EYIDOĞAN, H., and JACKSON, J. (1991b), *Source parameters of large earthquakes in the east Anatolian fault zone (Turkey)*, Geophys. J. Int. *106*, 537–550.

TODA, S., STEIN, R. S., REASENBERG, P. A., DIETERICH, P. H., and YOSHIDA, A. (1998), *Stress transfer by the 1995 $M_w = 6.9$ Kobe, Japan, shock: Effect of aftershocks and future earthquakes probabilities*, J. Geophys. Res. *103*, 24,543–24,565.

WELLS, D. L. and COPPERSMITH, K. J. (1994), *New empirical relationships among magnitude, rupture length, rupture width, rupture area and surface displacement*, Bull. Seismol. Soc. Am. *84*, 972–1002.

WESSEL, P. and SMITH, W. H. F. (1998), *New improved version of the Generic Mapping Tools Released*, EOS Trans. AGU *79*, 579.

WESTAWAY, R. (1990), *Block rotation in Western Turkey, 1. Observational evidence*, J. Geophys. Res. *95*, 19857–19884.

WESTAWAY, R. (1993), *Neogene evolution of the Denizli region of western Turkey*, J. Struct. Geol. *15*, 37–53.

(Received August 21, 2008, revised April 24, 2009, accepted June 18, 2009, Published online March 10, 2010)